European Journal of Mechanics / A Solids 79 (2020) 103871

Contents lists available at ScienceDirect

European Journal of Mechanics / A Solids

journal homepage: www.elsevier.com/locate/ejmsol

Shear locking in one-dimensional finite element methods

J.A. Baier-Saip [a,*], P.A. Baier [b], A.R. de Faria [c], J.C. Oliveira [d], H. Baier [e]

[a] Universidad Católica del Maule, Facultad de Ciencias Básicas, Av. San Miguel 3605, Casilla 617, Talca, Chile
[b] Instituto Federal de Educação, Ciência e Tecnologia do Ceará, Rua Estevão Remígio 1145, Limoeiro do Norte - CE, Brazil
[c] Instituto Tecnológico de Aeronáutica, Praça Marechal Eduardo Gomes 50, São José dos Campos - SP, Brazil
[d] Laboratório Nacional de Computação Científica, Av. Getúlio Vargas 333, Petrópolis - RJ, Brazil
[e] Universität Würzburg, am Hubland, 97074 Würzburg, Germany

ARTICLE INFO

Keywords:
Beam
Finite element methods
Shear locking

ABSTRACT

The accuracy of the results obtained with Finite Element Methods depends on the basis functions employed to approximate the displacement fields. If the beam is very thin, there can be shear locking and the numerical approximation leads to erroneous solutions. In this work, shear locking is analyzed by calculating expressly the curves of the transverse deflection, the cross-section rotation, and the shear strain in different approaches. The influence of the ratio between the shear stiffness and the bending stiffness is explicitly shown when force and moment loads are applied. It is concluded that the locking behavior at nodes is not the decisive factor to assess the quality of the solution. The important point is to analyze the entire curves when the ratio between the stiffnesses is varied. It is verified that the mixed interpolation and the discrete shear gap approaches are superior to the pure displacement and to the field consistency approaches.

1. Introduction

Shear locking (SL) is a well studied phenomenon in the conventional displacement approach of Finite Element Methods (FEM). The problem is caused by the use of the same interpolation functions for all the generalized displacement fields. When there is SL, the computations cannot reproduce the real behavior of slender structures (Leitão et al., 2007). Babuska and Suri (1992) provide a quantification of the tendency for finite elements to exhibit SL.

If transverse displacements are coupled with section rotations in Euler–Lagrangian equations and low order interpolations are adopted, then SL occurs (Yunhua, 1998), which is a significant problem when using FEM (Steiner et al., 2016). The increase of the degree of interpolation functions can alleviate the locking effects in traditional FEM, but it does not completely eliminate the SL (Garcia et al., 2000; Wong et al., 2018). The convergence rate of the approximation is not optimal as the number of nodes increases and gives rise to spurious oscillations in the shear forces (Prathap, 1993).

There are a number of possible ways to circumvent, or at least alleviate SL: (i) reduced/selective integration, (ii) mixed formulations, (iii) method of incompatible modes. More recently, a fourth method has been gaining popularity: the absolute nodal coordinate formulation (Shabana, 1997), originally proposed to accurately model large deformation and rotation effects in non-incremental type of solutions. It was soon realized that the technique could be successfully extended to handle locking problems and particularly SL (Dufva et al., 2005; García-Vallejo et al., 2007; Gerstmayr and Matikainen, 2006; Gerstmayr and Irschik, 2008; Gerstmayr et al., 2008, 2013; Nachbagauer et al., 2011, 2013; Valkeapää et al., 2015; Ebel et al., 2017).

The reduced integration approach proposed by Zienkiewicz et al. (1971) has been the preferred technique to alleviate SL. The mathematical foundations of this procedure were given later by Malkus and Hughes (1978) and it is based on the equivalence between the reduced integration (displacement-based) approach and certain mixed models. Noor and Peters (1981) discussed this equivalence further by comparing their stiffness matrices. The reduced integration approach can be interpreted as an efficient way to implement mixed methods.

Mixed methods have been extensively used in FEM for tackling issues like excessive bending stiffness (Patel and Shabana, 2018). With the MI, based on independent approximation of some interior fields, SL can be eliminated (Dolbow and Belytschko, 1998; De and Bathe, 2001). The MI will work correctly as long as the Ladyzhenskaya–Babuska–Brezzy stability criterion is satisfied. Moreover, by a change of the independent variables, it is possible to construct a locking-free approach (Cho and Atluri, 2001).

In the incompatible modes approach, the interpolation functions are enriched in order to achieve specific goals, e.g. to analytically represent the correct behavior under pure bending or to eliminate SL

* Corresponding author.
E-mail address: jbaier@ucm.cl (J.A. Baier-Saip).

https://doi.org/10.1016/j.euromechsol.2019.103871
Received 17 April 2019; Received in revised form 26 September 2019; Accepted 2 October 2019
Available online 4 October 2019

(Wilson et al., 1973; Wilson and Ibrahimbegovic, 1990; Bathe, 1996; de Sá et al., 2002; Sussman and Bathe, 2014). In comparison to traditional elements that do not rely on incompatible modes, these elements are not prone to SL and pass patch tests (Bazeley et al., 1966). A disadvantage of elements based on incompatible modes is that they may be unstable in large strain analyses (de Souza Neto et al., 1995; Wriggers and Reese, 1996; Pantuso and Bathe, 1997). These elements can also be viewed as an special case of the enhanced strain elements. As will become clear in the following sections, the key proposal of this work is the use of a pseudo-shear strain field that can also be interpreted as enhanced strain.

The present work is based on Timoshenko beam theory to represent the kinematics of deformation, which is equivalent to a shear deformable Reddy beam of infinite order (Polizzotto, 2015). The difference among diverse Timoshenko beam finite elements is in the choice of the interpolation functions used for the transverse deflection and rotation angle, or in the weak form to develop the model (Reddy, 1997). A reformulation of the classical Timoshenko beam was presented by Kiendl et al. (2018), resulting in a single differential equation. The isogeometric collocation scheme to solve the problem numerically is completely locking-free and they do not depend on the approximation degrees selected for the unknown fields (Veiga et al., 2012).

The SL origin in plate and shell elements can be traced back to the incapacity of those elements to accurately fulfill the requirement of null transverse shear strains and simultaneously maintain a minimal number of degrees of freedom to describe other modes of deformation (Zienkiewicz et al., 2013a,b). It is known that the null transverse shear strains condition is reached asymptotically as the thickness of the element goes to zero (Fox et al., 1993). The SL appears whenever the only mathematically possible solution is the one where no transverse deformations occur in the plate or shell element. In practice, as the thickness tends to zero, an unrealistic and dramatic increase of the element stiffness is observed.

Given the relevance of SL, alternative interpolation functions and schemes have been devised to hinder it. The most popular schemes derive from the Hu–Washizu principle, and consist in explicitly interpolating the transverse shear field using nodal midpoints on the edges of the element. The CQUAD4 element, initially developed by Macneal (1978) under the name of T1 element, is a good example of this type of scheme. Subsequently, other researchers sharpened and enhanced this element (Hughes and Tezduyar, 1981; Macneal, 1982; Dvorkin and Bathe, 1984).

Meshfree methods, based on moving least squares approximants, can be found in the literature (Belytschko et al., 1996; Liu et al., 1997). They have been applied in beam, plate, and shell analysis. Alternative meshfree methods, based on maximum-entropy approximants, have been introduced for the solution of problems in structural mechanics (Arroyo and Ortiz, 2006).

Other mixed approaches (Soh et al., 1999, 2001; Nguyen-Xuan, 2017) start from the Timoshenko's beam assumption and then develop plate elements which are free of SL. The SL observed in plates and shells is not addressed in the following sections. However, as an extension to higher dimensions, a curved beam is considered.

In order to analyze SL in one dimension, the curves of the transverse deflection, the cross-section rotation, and the shear strain are obtained within different approaches. Specifically, it is seen how the curves are modified when the ratio between the shear stiffness and the bending stiffness varies.

This paper is organized as follows. Initially, the beam equations are reviewed and the concept of pseudo shear strain is presented to differentiate from the conventional shear strain. Then the displacement fields when a cantilever is subjected to external loads (force and moment) are determined in different numerical approaches and they are compared with exact results. Typical features of the stiffness matrices are established and it is seen how the matrix in the PD can be decomposed. The calculations are carried out first with a varying number of nodes and thereafter the conclusions are generalized for increasing number of elements.

2. Methods

In the first part, the basic equations governing the deformation of beams are reviewed. Then the existence of the matrix inverse is established according to the linear dependence of the functions. At the end, the dimension of the basis to represent the pseudo shear strain is determined.

2.1. Review of beam equations

Consider a one-dimensional beam of length L subjected to force loads (of density = p) and to moment loads (of density = m). The beam has bending stiffness EI and shear stiffness kAG, where k represents the shear correction factor (a function of the cross-section geometry and of the Poisson ratio). The purpose is to determine the transverse deflection w and the cross-section rotation angle β of the beam as a function of the coordinate x. The boundary conditions are $w = 0$ and $\beta = 0$ at $x = 0$.

The static solution can be found using the principle of virtual work, which is equivalent to the minimization of the total potential energy

$$\Pi = \frac{1}{2} EI \int_0^L \left(\frac{\mathrm{d}\beta}{\mathrm{d}x}\right)^2 \mathrm{d}x + \frac{1}{2} kAG \int_0^L \gamma^2 \,\mathrm{d}x - \int_0^L pw \,\mathrm{d}x - \int_0^L m\beta \,\mathrm{d}x \quad (1)$$

The first integral represents the bending strain energy, the second integral represents the shearing strain energy, and the last two integrals represent the potential energy of the loads. Furthermore, the shear strain γ is given by

$$\gamma = \frac{\mathrm{d}w}{\mathrm{d}x} - \beta \quad (2)$$

In thin beams kAG is much bigger than EI/L^2 and the minimum occurs when γ is close to zero. Small "numerical errors" in the second integral of Eq. (1) are multiplied by a large number compared to the first integral, resulting in SL (Oesterle et al., 2018).

In order to obtain a numerical solution (NS), it is assumed that w and β can be approximated by polynomials. Using a basis $\mathcal{F}_N = \{f_i\}$ of dimension N, the transverse deflection and the rotation angle are written as

$$\begin{aligned} w &= \mathsf{f}_w^T \hat{\mathsf{u}} \\ \beta &= \mathsf{f}_\beta^T \hat{\mathsf{u}} \end{aligned} \quad (3)$$

where the vectors are defined by

$$\begin{aligned} \mathsf{f}_w^T &= \begin{pmatrix} f_1 & f_2 & \cdots & f_N & 0 & 0 & \cdots & 0 \end{pmatrix} \\ \mathsf{f}_\beta^T &= \begin{pmatrix} 0 & 0 & \cdots & 0 & f_1 & f_2 & \cdots & f_N \end{pmatrix} \\ \hat{\mathsf{u}}^T &= \begin{pmatrix} w_1 & w_2 & \cdots & w_N & \beta_1 & \beta_2 & \cdots & \beta_N \end{pmatrix} \end{aligned} \quad (3a)$$

Moreover, it is convenient to define

$$\begin{aligned} \mathsf{g}_w &= \frac{\mathrm{d}\mathsf{f}_w}{\mathrm{d}x} \\ \mathsf{g}_\beta &= \frac{\mathrm{d}\mathsf{f}_\beta}{\mathrm{d}x} \end{aligned} \quad (3b)$$

Considering an arbitrary variation $\delta\hat{\mathsf{u}}$, the condition for an extremum of Π in Eq. (1) results in the following linear system

$$\mathsf{K}\hat{\mathsf{u}} = \mathsf{p} + \mathsf{m} \quad (4)$$

where the stiffness matrix is given by

$$\mathsf{K} = EI \int_0^L \mathsf{g}_\beta \mathsf{g}_\beta^T \,\mathrm{d}x + kAG \int_0^L (\mathsf{g}_w - \mathsf{f}_\beta)(\mathsf{g}_w - \mathsf{f}_\beta)^T \,\mathrm{d}x \quad (4a)$$

and

$$\begin{aligned} \mathsf{p} &= \int_0^L p\mathsf{f}_w \,\mathrm{d}x \\ \mathsf{m} &= \int_0^L m\mathsf{f}_\beta \,\mathrm{d}x \end{aligned} \quad (4b)$$

2.2. Matrix inverse

Instead of the coordinate x, the basis functions are commonly written in terms of the dimensionless variable ξ. When there is only one element, the two variables are related by

$$x = L\frac{1+\xi}{2} \tag{5}$$

with $-1 \le \xi \le 1$. Hence, the Jacobian becomes

$$J = \frac{\mathrm{d}x}{\mathrm{d}\xi} = \frac{L}{2} \tag{6}$$

The accuracy of the NS depends on the dimension N of the space spanned by the basis. A convenient choice of basis functions is the Lagrange basis $\mathcal{F}_N = \{f_i(\xi)\}$ of degree $N_1 = N-1$. The Lagrange polynomials have the property

$$f_i(\xi_j) = \delta_{ij} \tag{7}$$

where δ_{ij} is the Kronecker delta and $\xi_1 < \xi_2 < \cdots < \xi_N$ are the nodes with $\xi_1 = -1$, $\xi_N = 1$. In this way, the coefficients w_i and β_i in Eq. (3a) are the values at $\xi = \xi_i$ of w and β respectively. Moreover, it can be shown that

$$f_1(\xi) + f_2(\xi) + \cdots + f_N(\xi) = 1 \tag{8}$$

for all ξ. In particular, if $w_1 = w_2 = \cdots = w_N = W$ (a constant) it follows that $w(\xi) = W$, i.e. a uniform translation results if each node is displaced by the same amount.

Lemma 1. *Let $\mathcal{R}_S = \{r_i(\xi)\}$ be a set of S functions and define*

$$R_{ij} = \int_{-1}^{1} r_i(\xi)\, r_j(\xi)\, \mathrm{d}\xi \tag{9}$$

The matrix R *has an inverse if, and only if, the set $\mathcal{R}_S$ is linearly independent.*

Proof. Consider the linear combination

$$c_1 r_1(\xi) + c_2 r_2(\xi) + \cdots + c_S r_S(\xi) = 0 \tag{10}$$

Multiplying Eq. (10) by $r_1(\xi)$ and integrating in the interval $[-1, 1]$, it follows that

$$c_1 R_{11} + c_2 R_{12} + \cdots + c_S R_{1S} = 0$$

Repeating this procedure with $r_2(\xi)$, $\cdots$, $r_S(\xi)$, a system of S linear homogeneous equations is obtained, which can be put in matrix form

$$\mathsf{R}\mathsf{c} = 0 \tag{11a}$$

where

$$\mathsf{R} = \begin{pmatrix} R_{11} & R_{12} & \cdots & R_{1S} \\ R_{12} & R_{22} & \cdots & R_{2S} \\ \vdots & \vdots & & \vdots \\ R_{1S} & R_{2S} & \cdots & R_{SS} \end{pmatrix} \quad \mathsf{c} = \begin{pmatrix} c_1 \\ c_2 \\ \vdots \\ c_S \end{pmatrix} \tag{11b}$$

Eq. (11a) admits a nontrivial solution $\mathsf{c} \neq 0$ if, and only if, the inverse R^{-1} does not exist. According to Eq. (10), if $\mathsf{c} \neq 0$ the set $\mathcal{R}_S$ is linearly dependent (LD). On the other hand, if $\mathsf{c} = 0$ is the unique solution of Eq. (11a), then the inverse R^{-1} must exist and in this case the set $\mathcal{R}_S$ is linearly independent (LI). □

The Lagrange basis $\mathcal{F}_N$ has N polynomials of degree N_1, which are LI. Deriving Eq. (8)

$$\frac{\mathrm{d}f_1}{\mathrm{d}\xi} + \frac{\mathrm{d}f_2}{\mathrm{d}\xi} + \cdots + \frac{\mathrm{d}f_N}{\mathrm{d}\xi} = 0$$

showing that the set $\mathcal{F}'_N = \{\mathrm{d}f_i/\mathrm{d}\xi\}$ is LD. However, it can be converted into a LI set $\mathcal{A}_{N_1} = \{\mathrm{d}f_i/\mathrm{d}\xi\}$ by eliminating one of the derivatives. In this way the matrix

$$\mathsf{A} = \begin{pmatrix} A_{11} & A_{12} & \cdots & A_{1N_1} \\ A_{12} & A_{22} & \cdots & A_{2N_1} \\ \vdots & \vdots & & \vdots \\ A_{1N_1} & A_{2N_1} & \cdots & A_{N_1N_1} \end{pmatrix} \tag{12a}$$

with

$$A_{ij} = \int_{-1}^{1} \frac{\mathrm{d}f_i}{\mathrm{d}\xi}\frac{\mathrm{d}f_j}{\mathrm{d}\xi}\,\mathrm{d}\xi \tag{12b}$$

has an inverse.

2.3. Pseudo shear strain

The pseudo shear strain γ_* is defined in the Lagrange basis $\mathcal{F}_{N_1} = \{f_{i*}(\xi)\}$ as follows (Bathe, 1996)

$$\gamma_*(\xi) = \sum_{i=1}^{N_1} \gamma_{i*} f_{i*}(\xi) \tag{13a}$$

where

$$\gamma_{i*} = J^{-1}\frac{\mathrm{d}w}{\mathrm{d}\xi} - \beta\Big|_{\xi=\xi_{i*}} = \sum_{j=2}^{N}\left[J^{-1} w_j \frac{\mathrm{d}f_j(\xi_{i*})}{\mathrm{d}\xi} - \beta_j f_j(\xi_{i*})\right] \tag{13b}$$

Remark that the sum in Eq. (13b) starts at $j = 2$ because according to the boundary conditions $w_1 = 0$ and $\beta_1 = 0$.

Inserting Eq. (13b) in Eq. (13a)

$$\begin{aligned}\gamma_*(\xi) &= \sum_{i=1}^{N_1}\sum_{j=2}^{N}\left[J^{-1} w_j \frac{\mathrm{d}f_j(\xi_{i*})}{\mathrm{d}\xi} - \beta_j f_j(\xi_{i*})\right] f_{i*}(\xi) \\ &= \sum_{j=2}^{N} J^{-1} w_j \psi_j(\xi) - \sum_{j=2}^{N} \beta_j \varphi_j(\xi)\end{aligned} \tag{14a}$$

where

$$\begin{aligned}\psi_j(\xi) &= \sum_{i=1}^{N_1} \frac{\mathrm{d}f_j(\xi_{i*})}{\mathrm{d}\xi} f_{i*}(\xi) \\ \varphi_j(\xi) &= \sum_{i=1}^{N_1} f_j(\xi_{i*}) f_{i*}(\xi)\end{aligned} \tag{14b}$$

It will now be shown why the dimension of the Lagrange basis used to expand the shear strain in Eq. (13a), can neither be greater nor lower than N_1.

Lemma 2. *Let $\mathcal{F}_S = \{f_i(\xi)\}$ be a Lagrange basis for polynomials of degree $S-1$. Consider a polynomial $q(\xi)$ defined by*

$$q(\xi) = \sum_{i=1}^{S} p(\xi_i)\, f_i(\xi) \tag{15}$$

where $p(\xi)$ is an arbitrary polynomial. If the degree of $p(\xi)$ is lower than S, then $p(\xi) = q(\xi)$, otherwise the polynomials are different.

Proof. Since the polynomial $q(\xi)$ is a linear combination of $f_i(\xi)$, it follows that the degree of $q(\xi)$ cannot be greater than $S-1$. Thus, when the degree of $p(\xi)$ is greater than or equal to S, the polynomials $p(\xi)$ and $q(\xi)$ are different.

Now consider the case when the degree of $p(\xi)$ is lower than S. Since the Lagrange polynomials have the property $f_i(\xi_j) = \delta_{ij}$, from Eq. (15) it follows that

$$q(\xi_j) = p(\xi_j)$$

for $j = 1, 2, \ldots, S$. Because the polynomials $p(\xi)$ and $q(\xi)$ are equal at S points and their degree is lower than S, they must be identical. □

The degree of the polynomials $f_i(\xi)$ in the Lagrange basis $\mathcal{F}_N$ is equal to N_1, and so the degree of $\mathrm{d}f_i/\mathrm{d}\xi$ is $N_1 - 1$. Moreover, the degree of $f_{i*}(\xi)$ in the Lagrange basis $\mathcal{F}_{N_1}$ is equal to $N_1 - 1$. From Eq. (14b) and Lemma 2, it follows that $\psi_j(\xi) = \mathrm{d}f_j/\mathrm{d}\xi$ and $\varphi_j(\xi) \neq f_j(\xi)$. In particular, the set $\{\psi_1, \psi_2, \ldots, \psi_{N_1}\}$ coincides with the set $\mathcal{A}_{N_1}$ and so the matrix $\boldsymbol{\Psi}$ defined by

$$\Psi_{ij} = \int_{-1}^{1} \psi_i(\xi)\psi_j(\xi)\,\mathrm{d}\xi \tag{16}$$

is equal to the matrix A (Eq. (12b)).

Lemma 3. *If the dimension N_+ of the Lagrange basis $\mathcal{F}_{N_+}$ is greater than N_1, then the pseudo shear strain γ_* becomes identical to the shear strain γ in the pure displacement approach.*

Proof. If $\mathcal{F}_{N_1}$ is replaced by $\mathcal{F}_N$, then $\psi_j(\xi) = \mathrm{d}f_j/\mathrm{d}\xi$ and $\varphi_j(\xi) = f_j(\xi)$ because the degree of the new Lagrange basis is $N - 1 = N_1$, which is greater than the degree of $\mathrm{d}f_j/\mathrm{d}\xi$ and equal to the degree of $f_j(\xi)$. Thus, using Eq. (14a)

$$\begin{aligned}\gamma_* &= \sum_{j=2}^{N} J^{-1} w_j \frac{\mathrm{d}f_j}{\mathrm{d}\xi} - \sum_{j=2}^{N} \beta_j f_j(\xi) \\ &= J^{-1} \frac{\mathrm{d}}{\mathrm{d}\xi} \sum_{j=2}^{N} w_j f_j(\xi) - \sum_{j=2}^{N} \beta_j f_j(\xi) \\ &= \frac{\mathrm{d}w}{\mathrm{d}x} - \beta = \gamma\end{aligned}$$

In general, this result holds if $\mathcal{F}_{N_1}$ is replaced by $\mathcal{F}_{N_+}$ for any $N_+ > N_1$. □

Therefore, when the number of tie points is greater than N_1, the functions used to evaluate the matrix integral representing the shear strain energy are the same functions as in the PD.

Lemma 4. *If the dimension N_- of the basis $\mathcal{F}_{N_-}$ is lower than N_1, then the matrix becomes singular.*

Proof. If $\mathcal{F}_{N_1}$ is replaced by $\mathcal{F}_{N_2}$ with $N_2 = N_1 - 1$, then the degree of the polynomials $\psi_i(\xi)$ will be $N_2 - 1 = N_1 - 2$. Hence, the set $\{\psi_1, \psi_2, \ldots, \psi_{N_1}\}$ is not LI and now the matrix $\boldsymbol{\Psi}$ of dimension $N_1 \times N_1$ defined in Eq. (16), does not have an inverse (Lemma 1). In general, $\boldsymbol{\Psi}$ will not have an inverse if $\mathcal{F}_{N_1}$ is replaced by $\mathcal{F}_{N_-}$ for any $N_- < N_1$, i.e. when the number of tie points is less than N_1. □

Since the matrix becomes singular when $N_- < N_1$, zero energy modes appear. Finally, from Lemmas 3 and 4 it is concluded that

Theorem 1. *The only way to obtain a feasible pseudo shear strain representation is to use N_1 tie points ξ_{i*} and a basis $\mathcal{F}_{N_1} = \{f_{i*}(\xi)\}$ for polynomials of degree $N_1 - 1$.*

In the reduced integration approach, using less points in the numerical integration is equivalent to decrease the degree of the polynomials being integrated. The effect is similar to change the basis from $\mathcal{F}_N$ to $\mathcal{F}_{N_1}$, where the degree of the polynomials decreases. Hence, the reduction in the integration order should be two, because the integrand is the product of two polynomials and the degree of each polynomial decreases by one.

3. Results

In order to analyze SL, a few basic results are reviewed and it is seen how SL manifests. In particular, the outcomes are discussed in terms of the dimensionless parameter α which measures the relative importance of the shear energy and of the bending energy. The calculations are carried out first with polynomials of degree one and then with polynomials of degree three. As an extension to higher dimensions, a curved beam with cubic interpolation of the displacements is considered. Distinctive features of the matrices in the PD and in the MI are established, and finally the results are generalized for an arbitrary number of elements.

3.1. Exact solution

The simplest example is a cantilever loaded with a force P and with a moment M (Fig. 1). In order to simplify the notation, the equations will be written using the dimensionless variable

$$y = \frac{x}{L} \tag{17}$$

When the loads are at the point $y = a$, the ES of the problem is

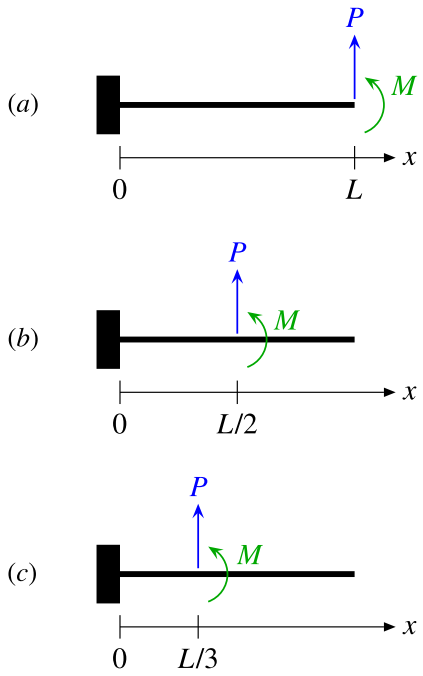

Fig. 1. Cantilever with applied force P and moment M (a) at the tip $x = L$, (b) at the center $x = L/2$, and (c) off-center at $x = L/3$.

- transverse deflection

$$w = \begin{cases} \dfrac{ML^2}{EI}\dfrac{y^2}{2} + \dfrac{PL^3}{EI}\left(\dfrac{ay^2}{2} - \dfrac{y^3}{6}\right) + \dfrac{PL}{kAG}y \\ \quad \text{for } 0 \le y \le a \\ \dfrac{ML^2}{EI}\left(ay - \dfrac{a^2}{2}\right) + \dfrac{PL^3}{EI}\left(\dfrac{a^2 y}{2} - \dfrac{a^3}{6}\right) + \dfrac{PL}{kAG}a \\ \quad \text{for } a < y \le 1 \end{cases} \tag{18a}$$

- rotation angle

$$\beta = \begin{cases} \dfrac{ML}{EI}y + \dfrac{PL^2}{EI}\left(ay - \dfrac{y^2}{2}\right) & \text{for } 0 \le y \le a \\ \dfrac{ML}{EI}a + \dfrac{PL^2}{EI}\dfrac{a^2}{2} & \text{for } a < y \le 1 \end{cases} \tag{18b}$$

- shear strain

$$\gamma = \begin{cases} \dfrac{P}{kAG} & \text{for } 0 \le y \le a \\ 0 & \text{for } a < y \le 1 \end{cases} \tag{18c}$$

In general, the functions $w(y)$ and $\beta(y)$ are continuous at $y = a$, but $\gamma(y)$ is discontinuous if $P \neq 0$. Furthermore, the derivatives $\mathrm{d}w/\mathrm{d}y$ and $\mathrm{d}\beta/\mathrm{d}y$ are discontinuous if $P \neq 0$ and $M \neq 0$ respectively. The ES is not an analytic function if $a \neq 1$ and the numerical approximation cannot give the ES with basis functions (polynomials) of any degree. Hence, the loads at $a = 1/2$ and at $a = 1/3$ are suitable to test the different NS.

The average values of w and β in the interval $0 < y < 1$ are for $a = 1$

$$\begin{aligned}\langle w \rangle &= \frac{ML^2}{6EI} + \frac{PL^3}{8EI} + \frac{PL}{2kAG} \\ \langle \beta \rangle &= \frac{ML}{2EI} + \frac{PL^2}{3EI}\end{aligned} \tag{19}$$

In particular, the limit of $\langle w \rangle$ when the shear rigidity becomes very small $kAG \ll EI/L^2$ is

$$\langle w \rangle \approx \frac{ML^2}{6EI} + \frac{PL}{2kAG} \tag{19a}$$

and when the shear rigidity becomes very large $kAG \gg EI/L^2$ is

$$\langle w \rangle \approx \frac{ML^2}{6EI} + \frac{PL^3}{8EI} \tag{19b}$$

The second case is the one of interest, because in thin beams $k \lesssim 1$, $G \lesssim E/2$, and $A \gg I/L^2$.

3.2. Two nodes analysis (tip load only)

In this section, the outcomes of the numerical approaches are given for the PD and for the MI when the basis is linear. In particular, it is seen how the shear energy changes between the two approaches.

3.2.1. Pure displacement

The Timoshenko beam finite element with linear interpolation of w and β is the simplest element. As remarked previously $w_1 = 0$, $\beta_1 = 0$, and so these components can be dropped from the vector $\hat{u}$ in Eq. (3a). In order to simplify the equations further, f_w, f_β, and $\hat{u}$ are replaced by

$$\mathsf{f}_{aw} = \begin{pmatrix} f_{a2} \\ 0 \end{pmatrix} \quad \mathsf{f}_{a\beta} = \begin{pmatrix} 0 \\ f_{a2} \end{pmatrix} \quad \hat{u}_a = \begin{pmatrix} u_{a1} \\ u_{a2} \end{pmatrix} = \begin{pmatrix} 2w_{a2}/L \\ \beta_{a2} \end{pmatrix} \tag{20}$$

where $f_{a2} = (1+\xi)/2 = y$ is a Lagrange polynomial of degree one. Moreover, the following dimensionless physical parameter is introduced

$$\alpha = \frac{kAGL^2}{4EI} \tag{21}$$

which can be linked to the parameter $\Omega = 1/4\alpha$ of Reddy (1997) or to the parameter $\phi = 3/\alpha$ of Friedman and Kosmatka (1993).

If the loads are applied at the tip, then

$$\mathsf{p}_a + \mathsf{m}_a = \begin{pmatrix} P \\ M \end{pmatrix}$$

and after a few algebraic manipulations Eq. (4) becomes

$$\begin{pmatrix} \frac{\alpha}{2} & -\frac{\alpha}{2} \\ -\frac{\alpha}{2} & \frac{1}{2} + \frac{2\alpha}{3} \end{pmatrix} \begin{pmatrix} u_{a1} \\ u_{a2} \end{pmatrix} = \begin{pmatrix} \frac{PL^2}{4EI} \\ \frac{ML}{2EI} \end{pmatrix} \tag{22}$$

Solving for u_{a1} and u_{a2}

$$u_{a1} = \frac{2w_{a2}}{L} = \frac{1}{\Delta_3}\left(\frac{ML}{EI} + \frac{2PL^2}{3EI} + \frac{PL^2}{2\alpha EI}\right)$$
$$u_{a2} = \beta_{a2} = \frac{1}{\Delta_3}\left(\frac{ML}{EI} + \frac{PL^2}{2EI}\right) \tag{23}$$

where, in general, Δ_η is defined by

$$\Delta_\eta = 1 + \frac{\alpha}{\eta} \tag{24}$$

Noting that $L^2/4\alpha EI = 1/kAG$, the curves calculated within the numerical approximation are

$$w_a = w_{a2} f_{a2} = \frac{1}{\Delta_3}\left(\frac{ML^2}{2EI} + \frac{PL^3}{3EI} + \frac{PL}{kAG}\right) y$$
$$\beta_a = \beta_{a2} f_{a2} = \frac{1}{\Delta_3}\left(\frac{ML}{EI} + \frac{PL^2}{2EI}\right) y \tag{25}$$

Furthermore,

$$\gamma_a = \frac{1}{L}\frac{\mathrm{d}w_a}{\mathrm{d}y} - \beta_a = \frac{1}{\Delta_3}\left(\frac{ML}{EI}\left[\frac{1}{2} - y\right] + \frac{PL^2}{EI}\left[\frac{1}{3} - \frac{y}{2}\right] + \frac{P}{kAG}\right) \tag{26}$$

Thus the averages are

$$\langle w_a \rangle = \frac{1}{\Delta_3}\left(\frac{ML^2}{4EI} + \frac{PL^3}{6EI} + \frac{PL}{2kAG}\right)$$
$$\langle \beta_a \rangle = \frac{1}{\Delta_3}\left(\frac{ML}{2EI} + \frac{PL^2}{4EI}\right) \tag{27}$$

On the one hand, for $kAG \ll EI/L^2$ i.e. $\alpha \to 0$ and $\Delta_3 \to 1$

$$\langle w_a \rangle \approx \frac{ML^2}{4EI} + \frac{PL}{2kAG}$$
$$\langle \beta_a \rangle \approx \frac{ML}{2EI} + \frac{PL^2}{4EI} \tag{27a}$$

which is of the same order of magnitude as in Eqs. (19) and (19a). On the other hand, for $kAG \gg EI/L^2$ i.e. $\alpha \gg 1$ and $\Delta_3 \approx \alpha/3$

$$\langle w_a \rangle \approx \frac{1}{\alpha}\left(\frac{3ML^2}{4EI} + \frac{PL^3}{2EI}\right)$$
$$\langle \beta_a \rangle \approx \frac{1}{\alpha}\left(\frac{3ML}{2EI} + \frac{3PL^2}{4EI}\right) \tag{27b}$$

which is much smaller than Eqs. (19) and (19b) by a factor of α. The approximation is poor and this phenomenon is known as SL. The locking is due to the inconsistency of the interpolations used for w_a and β_a, since a state of constant shear strain cannot be obtained if $\mathrm{d}w_a/\mathrm{d}y$ is a polynomial of degree zero and β_a is a polynomial of degree one (see Eq. (26)).

3.2.2. Mixed interpolation

To overcome locking, equal interpolations for both w_b and β_b may be used, but a lower-order polynomial of degree $N_1 - 1 = 0$ is used for the shear strain (Section 2.3). Specifically, γ_b is substituted by the pseudo shear strain

$$\gamma_{b*} = \mathsf{f}_{b\gamma*}^T \hat{u}_b \tag{28a}$$

with

$$\mathsf{f}_{b\gamma*} = \begin{pmatrix} \frac{1}{2} f_{b1*} \\ -\frac{1}{2} f_{b1*} \end{pmatrix} \quad \hat{u}_b = \begin{pmatrix} u_{b1} \\ u_{b2} \end{pmatrix} = \begin{pmatrix} 2w_{b2}/L \\ \beta_{b2} \end{pmatrix} \tag{28b}$$

and $f_{b1*} = 1$. Moreover, the stiffness matrix in Eq. (4a) is replaced by

$$\mathsf{K}_b = EI \int_0^L \mathsf{g}_{b\beta} \mathsf{g}_{b\beta}^T \,\mathrm{d}x + kAG \int_0^L \mathsf{f}_{b\gamma*} \mathsf{f}_{b\gamma*}^T \,\mathrm{d}x \tag{29}$$

and Eq. (22) is replaced by

$$\begin{pmatrix} \frac{\alpha}{2} & -\frac{\alpha}{2} \\ -\frac{\alpha}{2} & \frac{1}{2} + \frac{\alpha}{2} \end{pmatrix} \begin{pmatrix} u_{b1} \\ u_{b2} \end{pmatrix} = \begin{pmatrix} \frac{PL^2}{4EI} \\ \frac{ML}{2EI} \end{pmatrix} \tag{30}$$

Solving for u_{b1} and u_{b2}

$$u_{b1} = \frac{2w_{b2}}{L} = \frac{ML}{EI} + \frac{PL^2}{2EI} + \frac{PL^2}{2\alpha EI}$$
$$u_{b2} = \beta_{b2} = \frac{ML}{EI} + \frac{PL^2}{2EI} \tag{31}$$

Using $f_{b2} = f_{a2} = y$, the curves calculated within the numerical approximation are

$$w_b = w_{b2} f_{b2} = \left(\frac{ML^2}{2EI} + \frac{PL^3}{4EI} + \frac{PL}{kAG}\right) y$$
$$\beta_b = \beta_{b2} f_{b2} = \left(\frac{ML}{EI} + \frac{PL^2}{2EI}\right) y \tag{32}$$

and the averages are

$$\langle w_b \rangle = \frac{ML^2}{4EI} + \frac{PL^3}{8EI} + \frac{PL}{2kAG}$$
$$\langle \beta_b \rangle = \frac{ML}{2EI} + \frac{PL^2}{4EI} \tag{33}$$

The functions in Eq. (32) are different from Eqs. (18a) and (18b) when $a = 1$, mainly because the polynomial f_{b2} is only of degree one. However, the averages in Eq. (33) are of the same order as in Eq. (19) for $kAG \ll EI/L^2$ and also for $kAG \gg EI/L^2$.

Furthermore, from Eqs. (28a) and (28b)

$$\gamma_{b*} = \frac{w_{b2}}{L} - \frac{\beta_{b2}}{2} = \frac{P}{kAG} \tag{34a}$$

which is identical to the ES in Eq. (18c). In particular, the ES is a constant and so the polynomial f_{b1*} of degree zero is sufficient to fit the solution. On the other hand,

$$\gamma_b = \frac{1}{L}\frac{\mathrm{d}w_b}{\mathrm{d}y} - \beta_b = \gamma_{b*} + \left(\frac{ML}{EI} + \frac{PL^2}{2EI}\right)\left(\frac{1}{2} - y\right) \tag{34b}$$

Note that γ_{b*} is different from γ_b except at $y = 1/2$, the point at which it is tied.

3.2.3. Energy

It is interesting to compare the energy in the PD and in the MI. On the one hand, substituting $w_a = w_{a2} f_{a2}$ and $\beta_a = \beta_{a2} f_{a2}$ in Eq. (1), the potential energy becomes

$$\Pi_a = \frac{EI}{2L}\beta_{a2}^2 + \frac{kAGL}{2}\left(\frac{w_{a2}^2}{L^2} - \frac{w_{a2}}{L}\beta_{a2} + \frac{\beta_{a2}^2}{3}\right) - P w_{a2} - M\beta_{a2} \tag{35a}$$

On the other hand, substituting $w_b = w_{b2} f_{b2}$, $\beta_b = \beta_{b2} f_{b2}$, and $\gamma_{b*} = \gamma_{b1*} f_{b1*}$ in Eq. (1), the potential energy becomes

$$\Pi_b = \frac{EI}{2L}\beta_{b2}^2 + \frac{kAGL}{2}\left(\frac{w_{b2}}{L} - \frac{\beta_{b2}}{2}\right)^2 - P w_{b2} - M\beta_{b2} \tag{35b}$$

Putting $w_{a2} = w_{b2}$ and $\beta_{a2} = \beta_{b2} = \beta_0$, the difference between Π_a and Π_b is

$$\Pi_a - \Pi_b = \frac{kAGL}{24}\beta_0^2 \tag{35}$$

The bending energy remains the same but the shear energy decreases, so that a new equilibrium is found where shearing becomes less relevant.

In thin beams the shear strain energy is much bigger than the bending energy (Eq. (35a)) and the minimization forces both w_{a2}, β_{a2} to be very small, giving rise to SL in the PD. But in the MI a polynomial of degree zero is used to determine the shear strain, which is the same degree as the ES. Additionally, there is one degree of freedom to minimize the bending energy.

Although the NS is substantially improved in the MI, an accurate answer cannot be obtained with polynomials of degree one. Henceforth, the computations with linear basis functions will no longer be considered.

3.3. Cubic polynomials

A number of different approaches using polynomials of degree three as basis functions, can be employed to solve the problem. The difference is how the shear strain is calculated. With the purpose of comparing the approaches, the expansion coefficients and the curves are obtained for each one. Moreover, the concept of function locking (FL) is introduced, which will be used in the analysis.

3.3.1. Pure displacement

In order to have polynomials of degree three, the Lagrange basis $\mathcal{F}_4 = \{f_{ci}\}$ with nodes at $\xi_1 = -1$, $\xi_2 = -\frac{1}{3}$, $\xi_3 = \frac{1}{3}$, and $\xi_4 = 1$ is considered. The results of the calculations for three different cases, which include an applied force and an applied moment, are given below.

1c Tip load $a = 1$

The calculated expansion coefficients are

$$\begin{aligned}
u_{c1} &= \frac{2w_{c2}}{L} = \frac{ML}{9EI} + \frac{8PL^2}{81EI} + \frac{PL^2}{6\alpha EI}\\
u_{c2} &= \frac{2w_{c3}}{L} = \frac{4ML}{9EI} + \frac{28PL^2}{81EI} + \frac{PL^2}{3\alpha EI}\\
u_{c3} &= \frac{2w_{c4}}{L} = \frac{ML}{EI} + \frac{2PL^2}{3EI} + \frac{PL^2}{2\alpha EI}\\
u_{c4} &= \beta_{c2} = \frac{ML}{3EI} + \frac{5PL^2}{18EI}\\
u_{c5} &= \beta_{c3} = \frac{2ML}{3EI} + \frac{4PL^2}{9EI}\\
u_{c6} &= \beta_{c4} = \frac{ML}{EI} + \frac{PL^2}{2EI}
\end{aligned} \tag{36}$$

Substituting Eq. (36) in

$$\begin{aligned}
w_c &= w_{c2} f_{c2} + w_{c3} f_{c3} + w_{c4} f_{c4}\\
\beta_c &= \beta_{c2} f_{c2} + \beta_{c3} f_{c3} + \beta_{c4} f_{c4}
\end{aligned}$$

reproduces Eqs. (18a) and (18b) when $a = 1$. Furthermore, calculating

$$\gamma_c = \frac{1}{L}\frac{\mathrm{d}w_c}{\mathrm{d}y} - \beta_c$$

agrees with the exact shear strain (see Eq. (18c)).

2c Center load $a = 1/2$

The calculated expansion coefficients are

$$\begin{aligned}
u_{c1} &= \frac{2w_{c2}}{L} = \frac{13ML}{108EI} + \frac{23PL^2}{648EI} + \left(13 - \frac{7}{\Delta_{35}}\right)\frac{PL^2}{36\alpha EI}\\
u_{c2} &= \frac{2w_{c3}}{L} = \frac{11ML}{27EI} + \frac{19PL^2}{162EI} + \left(16 - \frac{7}{\Delta_{35}}\right)\frac{PL^2}{36\alpha EI}\\
u_{c3} &= \frac{2w_{c4}}{L} = \frac{3ML}{4EI} + \frac{5PL^2}{24EI} + \frac{PL^2}{4\alpha EI}\\
u_{c4} &= \beta_{c2} = \frac{ML}{3EI} + \left(\frac{7}{2} + \frac{1}{3\Delta_{35}}\right)\frac{PL^2}{36EI}\\
u_{c5} &= \beta_{c3} = \frac{ML}{2EI} + \left(5 - \frac{1}{3\Delta_{35}}\right)\frac{PL^2}{36EI}\\
u_{c6} &= \beta_{c4} = \frac{ML}{2EI} + \frac{PL^2}{8EI}
\end{aligned} \tag{37a}$$

where Δ_{35} is defined by Eq. (24) with $\eta = 35$. Moreover, the curves are

$$\begin{aligned}
w_c &= \frac{ML^2}{4EI}\left(\frac{5y^2}{2} - y^3\right) + \frac{PL^3}{4EI}\left(\frac{3y^2}{4} - \frac{y^3}{3}\right)\\
&\quad + \frac{PL}{kAG}\left(3y - \frac{5y^2}{2} - \frac{7}{4\Delta_{35}}\left[y - y^2\right]\right)\\
\beta_c &= \frac{ML}{4EI}(5y - 3y^2) + \frac{PL^2}{4EI}\left(\frac{3y}{2} - y^2 + \frac{1}{\Delta_{35}}\left[\frac{y}{2} - \frac{3y^2}{2} + y^3\right]\right)\\
\gamma_c &= -\frac{PL^2}{4EI}\frac{1}{\Delta_{35}}\left[\frac{y}{2} - \frac{3y^2}{2} + y^3\right] + \frac{P}{kAG}\left(3 - 5y - \frac{7}{4\Delta_{35}}\left[1 - 2y\right]\right)
\end{aligned} \tag{37b}$$

3c Off-center load $a = 1/3$

The calculated expansion coefficients are

$$\begin{aligned}
u_{c1} &= \frac{2w_{c2}}{L} = \left(23 + \frac{4}{\Delta_{35}}\right)\frac{ML}{243EI} + \frac{38PL^2}{2187EI} + \left(\frac{461}{18} - \frac{14}{\Delta_{35}}\right)\frac{PL^2}{81\alpha EI}\\
u_{c2} &= \frac{2w_{c3}}{L} = \left(76 + \frac{4}{\Delta_{35}}\right)\frac{ML}{243EI} + \frac{124PL^2}{2187EI} + \left(\frac{251}{9} - \frac{14}{\Delta_{35}}\right)\frac{PL^2}{81\alpha EI}\\
u_{c3} &= \frac{2w_{c4}}{L} = \frac{5ML}{9EI} + \frac{8PL^2}{81EI} + \frac{PL^2}{6\alpha EI}\\
u_{c4} &= \beta_{c2} = \left(7 + \frac{20}{27\Delta_{35}}\right)\frac{ML}{27EI} + \left(\frac{23}{2} + \frac{2}{\Delta_{35}}\right)\frac{PL^2}{243EI}\\
u_{c5} &= \beta_{c3} = \left(10 - \frac{20}{27\Delta_{35}}\right)\frac{ML}{27EI} + \left(16 - \frac{2}{\Delta_{35}}\right)\frac{PL^2}{243EI}\\
u_{c6} &= \beta_{c4} = \frac{ML}{3EI} + \frac{PL^2}{18EI}
\end{aligned} \tag{38a}$$

and the curves are

$$\begin{aligned}
w_c &= \frac{ML^2}{EI}\left(\frac{y^2}{2} - \frac{2y^3}{9} + \frac{1}{27\Delta_{35}}\left[y - y^2\right]\right) + \frac{PL^3}{54EI}\left(5y^2 - \frac{7y^3}{3}\right)\\
&\quad + \frac{PL}{27kAG}\left(79y - 90y^2 + 20y^3 - \frac{42}{\Delta_{35}}\left[y - y^2\right]\right)\\
\beta_c &= \frac{ML}{EI}\left(y - \frac{2y^2}{3} + \frac{10}{27\Delta_{35}}\left[y - 3y^2 + 2y^3\right]\right)\\
&\quad + \frac{PL^2}{54EI}\left(10y - 7y^2 + \frac{6}{\Delta_{35}}\left[y - 3y^2 + 2y^3\right]\right)\\
\gamma_c &= \frac{ML}{EI}\frac{1}{27\Delta_{35}}\left[1 - 12y + 30y^2 - 20y^3\right] - \frac{PL^2}{EI}\frac{1}{9\Delta_{35}}\left[y - 3y^2 + 2y^3\right]\\
&\quad + \frac{P}{27kAG}\left(79 - 180y + 60y^2 - \frac{42}{\Delta_{35}}\left[1 - 2y\right]\right)
\end{aligned} \tag{38b}$$

3.3.2. Mixed interpolation

In the MI the shear strain γ is replaced by the pseudo shear strain γ_* of Section 2.3. Since the dimension of the set $\{f_{di*}\}$ to represent γ_*

must be $N_1 = 4 - 1 = 3$ (Theorem 1), the three tie points are chosen at $\xi_{1*} = -\frac{2}{3}$, $\xi_{2*} = 0$, and $\xi_{3*} = \frac{2}{3}$.

1d Tip load $a = 1$

The coefficients u_{di} are equal to u_{ci} in Eq. (36) and, as before, the curves w_d, β_d coincide with the ES. Furthermore, γ_{dj*} is a linear combination of u_{di} and substituting γ_{dj*} in

$$\gamma_{d*} = \gamma_{d1*} f_{d1*} + \gamma_{d2*} f_{d2*} + \gamma_{d3*} f_{d3*} \tag{39}$$

reproduces Eq. (18c) when $a = 1$. Hence, $\gamma_{d*} = \gamma_d$ not only at the tie points but in the whole interval $-1 \le \xi \le 1$.

Note that if the tie points are replaced by the usual Gauss points $\xi_{G1*} = -\sqrt{\frac{3}{5}}$, $\xi_{G2*} = 0$, and $\xi_{G3*} = \sqrt{\frac{3}{5}}$, then the same curves are obtained.

2d Center load $a = 1/2$

The calculated expansion coefficients are

$$\begin{aligned}
u_{d1} &= \frac{2w_{d2}}{L} = \frac{13ML}{108EI} + \frac{539PL^2}{11664EI} + \frac{PL^2}{6\alpha EI}\\
u_{d2} &= \frac{2w_{d3}}{L} = \frac{11ML}{27EI} + \frac{1493PL^2}{11664EI} + \frac{PL^2}{4\alpha EI}\\
u_{d3} &= \frac{2w_{d4}}{L} = \frac{3ML}{4EI} + \frac{5PL^2}{24EI} + \frac{PL^2}{4\alpha EI}\\
u_{d4} &= \beta_{d2} = \frac{ML}{3EI} + \frac{107PL^2}{972EI}\\
u_{d5} &= \beta_{d3} = \frac{ML}{2EI} + \frac{245PL^2}{1944EI}\\
u_{d6} &= \beta_{d4} = \frac{ML}{2EI} + \frac{PL^2}{8EI}
\end{aligned} \tag{40a}$$

and the curves are

$$\begin{aligned}
w_d &= \frac{ML^2}{4EI}\left(\frac{5y^2}{2} - y^3\right) + \frac{PL^3}{12EI}\left(\frac{125y}{432} + \frac{847y^2}{432} - y^3\right)\\
&\quad + \frac{PL}{4kAG}(5y - 3y^2)\\
\beta_d &= \frac{ML}{4EI}(5y - 3y^2) + \frac{PL^2}{12EI}\left(\frac{79y}{12} - \frac{37y^2}{4} + \frac{25y^3}{6}\right)\\
\gamma_{d*} &= \frac{P}{4kAG}(5 - 6y)\\
\gamma_d &= \gamma_{d*} + \frac{25PL^2}{72EI}\left(\frac{1}{6} - y\right)\left(\frac{1}{2} - y\right)\left(\frac{5}{6} - y\right)
\end{aligned} \tag{40b}$$

If the tie points are the Gauss points ξ_{G1*}, ξ_{G2*}, ξ_{G3*}, then $\gamma_{G*} = \gamma_{d*}$ (Eq. (40b)) but the other curves are slightly different

$$\begin{aligned}
w_G &= \frac{ML^2}{4EI}\left(\frac{5y^2}{2} - y^3\right) + \frac{PL^3}{12EI}\left(\frac{3y}{20} + \frac{21y^2}{10} - y^3\right) + \frac{PL}{4kAG}(5y - 3y^2)\\
\beta_G &= \frac{ML}{4EI}(5y - 3y^2) + \frac{PL^2}{12EI}\left(6y - \frac{15y^2}{2} + 3y^3\right)\\
\gamma_G &= \gamma_{G*} + \frac{PL^2}{4EI}\left(\frac{1}{2}\left[1 - \sqrt{\frac{3}{5}}\right] - y\right)\left(\frac{1}{2} - y\right)\left(\frac{1}{2}\left[1 + \sqrt{\frac{3}{5}}\right] - y\right)
\end{aligned} \tag{41}$$

A calculation reveals that the deviation of w_G to the exact transverse deflection curve is smaller than the deviation of w_d. But the deviation of β_G to the exact rotation angle curve is bigger than the deviation of β_d.

3d Off-center load $a = 1/3$

The calculated expansion coefficients are

$$\begin{aligned}
u_{d1} &= \frac{2w_{d2}}{L} = \frac{257ML}{2187EI} + \frac{353PL^2}{13122EI} + \frac{209PL^2}{1458\alpha EI}\\
u_{d2} &= \frac{2w_{d3}}{L} = \frac{734ML}{2187EI} + \frac{869PL^2}{13122EI} + \frac{125PL^2}{729\alpha EI}\\
u_{d3} &= \frac{2w_{d4}}{L} = \frac{5ML}{9EI} + \frac{8PL^2}{81EI} + \frac{PL^2}{6\alpha EI}\\
u_{d4} &= \beta_{d2} = \frac{209ML}{729EI} + \frac{257PL^2}{4374EI}\\
u_{d5} &= \beta_{d3} = \frac{250ML}{729EI} + \frac{119PL^2}{2187EI}
\end{aligned}$$

$$u_{d6} = \beta_{d4} = \frac{ML}{3EI} + \frac{PL^2}{18EI} \tag{42a}$$

and the curves are

$$\begin{aligned}
w_d &= \frac{ML^2}{9EI}\left(\frac{25y}{54} + \frac{109y^2}{27} - 2y^3\right) + \frac{PL^3}{27EI}\left(\frac{125y}{216} + \frac{415y^2}{216} - \frac{7y^3}{6}\right)\\
&\quad + \frac{PL}{9kAG}\left(\frac{37y}{3} - 16y^2 + \frac{20y^3}{3}\right)\\
\beta_d &= \frac{ML}{9EI}\left(\frac{37y}{3} - 16y^2 + \frac{20y^3}{3}\right) + \frac{PL^2}{27EI}\left(\frac{55y}{6} - 16y^2 + \frac{25y^3}{3}\right)\\
\gamma_{d*} &= \frac{P}{9kAG}\left(\frac{37}{3} - 32y + 20y^2\right)\\
\gamma_d &= \gamma_{d*} + \left(\frac{20ML}{27EI} + \frac{25PL^2}{81EI}\right)\left(\frac{1}{6} - y\right)\left(\frac{1}{2} - y\right)\left(\frac{5}{6} - y\right)
\end{aligned} \tag{42b}$$

Finally, if the tie points are the Gauss points ξ_{G1*}, ξ_{G2*}, ξ_{G3*}, then $\gamma_{G*} = \gamma_{d*}$ (Eq. (42b)) but the other curves are slightly different

$$\begin{aligned}
w_G &= \frac{ML^2}{9EI}\left(\frac{y}{3} + \frac{25y^2}{6} - 2y^3\right) + \frac{PL^3}{27EI}\left(\frac{3y}{10} + \frac{11y^2}{5} - \frac{7y^3}{6}\right)\\
&\quad + \frac{PL}{9kAG}\left(\frac{37y}{3} - 16y^2 + \frac{20y^3}{3}\right)\\
\beta_G &= \frac{ML}{9EI}\left(\frac{37y}{3} - 16y^2 + \frac{20y^3}{3}\right) + \frac{PL^2}{27EI}\left(8y - \frac{25y^2}{2} + 6y^3\right)\\
\gamma_G &= \gamma_{G*} + \left(\frac{20ML}{27EI} + \frac{2PL^2}{9EI}\right)\left(\frac{1}{2}\left[1 - \sqrt{\frac{3}{5}}\right] - y\right)\\
&\quad \times \left(\frac{1}{2} - y\right)\left(\frac{1}{2}\left[1 + \sqrt{\frac{3}{5}}\right] - y\right)
\end{aligned} \tag{43}$$

A calculation reveals that the deviations of w_G and β_G to the exact curves are smaller than the deviations of w_d and β_d. Indeed, the Gauss points (actually called Barlow points) usually provide the best accuracy when computing the strain (Carrera et al., 2017).

3.3.3. Field consistency

An approach based on a two-node Timoshenko beam was developed by Friedman and Kosmatka (1993). The method is equivalent to the field consistency (FC) approach introduced later by Yunhua (1998). It uses four cubic basis functions h_{wi} to expand the transverse deflection w, which is the same degree of the ES when the cantilever is loaded at the tip. Furthermore, it uses four quadratic basis functions $h_{\beta i}$ to expand the rotation angle β, which also coincides with the degree of the ES.

Specifically, the displacement fields are given by

$$\begin{aligned}
w_e &= w_{e1}h_{w1} + w_{e2}h_{w2} + \frac{L}{2}\beta_{e1}h_{w3} + \frac{L}{2}\beta_{e2}h_{w4}\\
\beta_e &= \frac{2}{L}w_{e1}h_{\beta 1} + \frac{2}{L}w_{e2}h_{\beta 2} + \beta_{e1}h_{\beta 3} + \beta_{e2}h_{\beta 4}
\end{aligned} \tag{44}$$

where the factors $L/2$ and $2/L$ have been introduced in order to make h_{w3}, h_{w4} and $h_{\beta 1}$, $h_{\beta 2}$ dimensionless. Using the variable ξ instead of x and replacing $\phi \to 3/\alpha$, the basis functions read

$$\begin{aligned}
h_{w1} &= \frac{1}{\Delta_3}\frac{1-\xi}{2}\left(1 + \alpha\frac{2 - \xi - \xi^2}{6}\right)\\
h_{w2} &= \frac{1}{\Delta_3}\frac{1+\xi}{2}\left(1 + \alpha\frac{2 + \xi - \xi^2}{6}\right)\\
h_{w3} &= \frac{1}{\Delta_3}\frac{1-\xi^2}{4}\left(1 + \alpha\frac{1-\xi}{3}\right)\\
h_{w4} &= -\frac{1}{\Delta_3}\frac{1-\xi^2}{4}\left(1 + \alpha\frac{1+\xi}{3}\right)
\end{aligned} \tag{44a}$$

In the limit $\alpha \to \infty$ the functions become the Hermite cubics. Furthermore,

$$\begin{aligned}
h_{\beta 1} &= -\frac{\alpha}{\Delta_3}\frac{1-\xi^2}{4}\\
h_{\beta 2} &= \frac{\alpha}{\Delta_3}\frac{1-\xi^2}{4}
\end{aligned}$$

$$h_{\beta 3} = \frac{1}{\Delta_3}\frac{1-\xi}{2}\left(1-\alpha\frac{1+3\xi}{6}\right)$$
$$h_{\beta 4} = \frac{1}{\Delta_3}\frac{1+\xi}{2}\left(1-\alpha\frac{1-3\xi}{6}\right) \tag{44b}$$

At the borders $\xi = \pm 1$ the basis functions do not depend on α. But inside the open interval $-1 < \xi < 1$ the basis functions depend on the parameter α which incorporates element material properties. Moreover, the functions contain the denominator Δ_3 which also appears in the PD when two nodes are considered (Section 3.2.1).

The boundary conditions at $\xi = -1$ are $w_e = w_{e1} = 0$ and $\beta_e = \beta_{e1} = 0$. As before, three loads are considered.

1e Tip load $a = 1$

The calculated expansion coefficients are

$$u_{e1} = \frac{2w_{e2}}{L} = \frac{ML}{EI} + \frac{2PL^2}{3EI} + \frac{PL^2}{2\alpha EI}$$
$$u_{e2} = \beta_{e2} = \frac{ML}{EI} + \frac{PL^2}{2EI} \tag{45}$$

and the curves coincide with the ES in Eqs. (18a)–(18c) when $a = 1$.

2e Center load $a = 1/2$

The calculated expansion coefficients are

$$u_{e1} = \frac{2w_{e2}}{L} = \frac{3ML}{4EI} + \frac{5PL^2}{24EI} + \frac{PL^2}{4\alpha EI}$$
$$u_{e2} = \beta_{e2} = \frac{ML}{2EI} + \frac{PL^2}{8EI} \tag{46a}$$

and the curves are

$$w_e = \frac{ML^2}{4EI}\left(\frac{5y^2}{2} - y^3 + \frac{1}{\Delta_3}\left[\frac{y}{2} - \frac{3y^2}{2} + y^3\right]\right) + \frac{PL^3}{4EI}\left(\frac{3y^2}{4} - \frac{y^3}{3}\right) + \frac{PL}{2kAG}y$$
$$\beta_e = \frac{ML}{4EI}\left(5y - 3y^2 - \frac{3}{\Delta_3}\left[y - y^2\right]\right) + \frac{PL^2}{4EI}\left(\frac{3y}{2} - y^2\right)$$
$$\gamma_e = \frac{ML}{EI}\frac{1}{8\Delta_3} + \frac{P}{2kAG} \tag{46b}$$

3e Off-center load $a = 1/3$

The calculated expansion coefficients are

$$u_{e1} = \frac{2w_{e2}}{L} = \frac{5ML}{9EI} + \frac{8PL^2}{81EI} + \frac{PL^2}{6\alpha EI}$$
$$u_{e2} = \beta_{e2} = \frac{ML}{3EI} + \frac{PL^2}{18EI} \tag{47a}$$

and the curves are

$$w_e = \frac{ML^2}{3EI}\left(\frac{3y^2}{2} - \frac{2y^3}{3} + \frac{1}{\Delta_3}\left[\frac{y}{3} - y^2 + \frac{2y^3}{3}\right]\right) + \frac{PL^3}{27EI}\left(\frac{5y^2}{2} - \frac{7y^3}{6} + \frac{1}{\Delta_3}\left[\frac{y^2}{2} - \frac{y^3}{3}\right]\right) + \frac{PL}{27kAG}\left(7y + \frac{2}{\Delta_3}[y]\right)$$
$$\beta_e = \frac{ML}{3EI}\left(3y - 2y^2 - \frac{2}{\Delta_3}\left[y - y^2\right]\right) + \frac{PL^2}{27EI}\left(5y - \frac{7y^2}{2} + \frac{1}{\Delta_3}\left[y - y^2\right]\right)$$
$$\gamma_e = \frac{ML}{EI}\frac{1}{9\Delta_3} + \frac{P}{27kAG}\left(7 + \frac{2}{\Delta_3}\right) \tag{47b}$$

3.3.4. Discrete shear gap

Bletzinger et al. (2000) introduced the discrete shear gap (DSG) approach, which results in locking free finite elements. The pseudo shear strain is given by

$$\gamma_* = \sum_{i=2}^{N} \Delta w_{\gamma i}\, J^{-1}\, \frac{\mathrm{d}f_i}{\mathrm{d}\xi} \tag{48a}$$

with

$$\Delta w_{\gamma i} = w_i - w_1 - \int_{r_1}^{r_i} \sum_{j=1}^{N} \beta_j f_j(\xi)\, J\, \mathrm{d}\xi \tag{48b}$$

The shear gap $\Delta w_{\gamma i}$ at node ξ_i represents the difference between the actual displacement $w_i - w_1$ and the displacement resulting from pure bending (Wong and Sugianto, 2017).

1f Tip load $a = 1$

The calculated expansion coefficients u_{fi} are identical to u_{ci} (Eq. (36)) and the curves coincide again with the ES.

2f Center load $a = 1/2$

The calculated expansion coefficients are

$$u_{f1} = \frac{2w_{f2}}{L} = \frac{13ML}{108EI} + \frac{247PL^2}{5832EI} + \frac{PL^2}{6\alpha EI}$$
$$u_{f2} = \frac{2w_{f3}}{L} = \frac{11ML}{27EI} + \frac{181PL^2}{1458EI} + \frac{PL^2}{4\alpha EI}$$
$$u_{f3} = \frac{2w_{f4}}{L} = \frac{3ML}{4EI} + \frac{5PL^2}{24EI} + \frac{PL^2}{4\alpha EI}$$
$$u_{f4} = \beta_{f2} = \frac{ML}{3EI} + \frac{209PL^2}{1944EI}$$
$$u_{f5} = \beta_{f3} = \frac{ML}{2EI} + \frac{125PL^2}{972EI}$$
$$u_{f6} = \beta_{f4} = \frac{ML}{2EI} + \frac{PL^2}{8EI} \tag{49a}$$

and the curves are

$$w_f = \frac{ML^2}{4EI}\left(\frac{5y^2}{2} - y^3\right) + \frac{PL^3}{12EI}\left(\frac{5y}{27} + \frac{223y^2}{108} - y^3\right) + \frac{PL}{4kAG}(5y - 3y^2)$$
$$\beta_f = \frac{ML}{4EI}(5y - 3y^2) + \frac{PL^2}{12EI}\left(\frac{37y}{6} - 8y^2 + \frac{10y^3}{3}\right)$$
$$\gamma_{f*} = \frac{P}{4kAG}(5 - 6y)$$
$$\gamma_f = \gamma_{f*} + \frac{5PL^2}{18EIL}\left(\frac{1}{2}\left[1 - \frac{\sqrt{5}}{3}\right] - y\right)\left(\frac{1}{2} - y\right)\left(\frac{1}{2}\left[1 + \frac{\sqrt{5}}{3}\right] - y\right) \tag{49b}$$

3f Off-center load $a = 1/3$

The calculated expansion coefficients are

$$u_{f1} = \frac{2w_{f2}}{L} = \frac{247ML}{2187EI} + \frac{154PL^2}{6561EI} + \frac{209PL^2}{1458\alpha EI}$$
$$u_{f2} = \frac{2w_{f3}}{L} = \frac{724ML}{2187EI} + \frac{412PL^2}{6561EI} + \frac{125PL^2}{729\alpha EI}$$
$$u_{f3} = \frac{2w_{f4}}{L} = \frac{5ML}{9EI} + \frac{8PL^2}{81EI} + \frac{PL^2}{6\alpha EI}$$
$$u_{f4} = \beta_{f2} = \frac{209ML}{729EI} + \frac{247PL^2}{4374EI}$$
$$u_{f5} = \beta_{f3} = \frac{250ML}{729EI} + \frac{124PL^2}{2187EI}$$
$$u_{f6} = \beta_{f4} = \frac{ML}{3EI} + \frac{PL^2}{18EI} \tag{50a}$$

and the curves are

$$w_f = \frac{ML^2}{9EI}\left(\frac{10y}{27} + \frac{223y^2}{54} - 2y^3\right) + \frac{PL^3}{81EI}\left(\frac{10y}{9} + \frac{115y^2}{18} - \frac{7y^3}{2}\right) + \frac{PL}{9kAG}\left(\frac{37y}{3} - 16y^2 + \frac{20y^3}{3}\right)$$
$$\beta_f = \frac{ML}{9EI}\left(\frac{37y}{3} - 16y^2 + \frac{20y^3}{3}\right) + \frac{PL^2}{81EI}\left(25y - \frac{81y^2}{2} + 20y^3\right)$$
$$\gamma_{f*} = \frac{P}{9kAG}\left(\frac{37}{3} - 32y + 20y^2\right)$$
$$\gamma_f = \gamma_{f*} + \left(\frac{20ML}{27EI} + \frac{20PL^2}{81EI}\right)\left(\frac{1}{2}\left[1 - \frac{\sqrt{5}}{3}\right] - y\right) \times \left(\frac{1}{2} - y\right)\left(\frac{1}{2}\left[1 + \frac{\sqrt{5}}{3}\right] - y\right) \tag{50b}$$

3.3.5. Analysis

Tip load. In cases **1c**, **1d**, **1e**, and **1f**, the NS always coincides with the ES. The key point is that the basis functions are polynomials of degree

three, which is the same degree of the ES for w. Any basis of degree three gives invariably the same result, i.e. the specific choice of the basis functions is not relevant. Furthermore, the basis functions for β are polynomials of degree two or three, which is equal to or greater than the degree of the ES. Finally, the shear strain is a polynomial of degree zero and, for example in the case of the MI, a basis of degree two as $\{f_{d1*}, f_{d2*}, f_{d3*}\}$ is sufficient to match the ES.

Coefficients. The coefficients $u_{\lambda i}$ ($\lambda = c, d, e, f$) are linear combinations of ML/EI, PL^2/EI, and $PL^2/\alpha EI = 4P/kAG$. Since a pure moment cannot generate a shear strain and the shear modulus G is associated with the shear strain, $ML/\alpha EI = 4M/kAGL$ shall never appear (see however Eq. (23) in the limit $\alpha \gg 1$, where linear basis functions have been used).

In the MI ($\lambda = d$), in the FC ($\lambda = e$), and in the DSG ($\lambda = f$) the coefficients $u_{\lambda i}$ do not depend on Δ_{35}. Furthermore, in the PD the coefficients $u_{c3} = 2w_{c4}/L$ (the transverse deflection at the tip) and $u_{c6} = \beta_{c4}$ (the rotation angle at the tip) do not depend on Δ_{35}. In general, using polynomials of degree three or higher, the transverse deflection and the rotation angle at the tip never depend on Δ_{35} (there is no SL at the borders of an element). But, for example in Eq. (37a), the number multiplying PL^2/EI in $u_{c4} = \beta_{c2}$ (the rotation angle at $x = L/3$) changes from $\left(\frac{7}{2} + \frac{1}{3}\right)\frac{1}{36} = \frac{23}{216}$ to $\frac{7}{2}\frac{1}{36} = \frac{7}{72}$ as Δ_{35} varies between 1 and ∞.

Curves. The exact shear strain is independent of the moment M. However, ML/EI appears in the shear strain of the PD (Eq. (38b)) and of the FC (Eqs. (46b) and (47b)). Although the moment also appears in the shear strain γ of the MI (Eq. (42b)) and of the DSG (Eq. (50b)), it never appears in γ_* which is the meaningful shear strain.

The polynomials in the square brackets of Eqs. (37b) and (38b) corresponding to the PD, are suppressed as the denominator $\Delta_{35} \to \infty$. For example, the polynomial multiplying PL^2/EI in the expansion of β_c in Eq. (37b), changes from $\frac{y}{2} - \frac{5y^2}{8} + \frac{y^3}{4}$ to $\frac{3y}{8} - \frac{y^2}{4}$ as Δ_{35} varies from 1 to ∞. The phenomenon is not as striking as in Eq. (25), where β_a changes from $\left(\frac{ML}{EI} + \frac{PL^2}{2EI}\right)y$ to 0.

Furthermore, the polynomials in the square brackets of the curves w_c and β_c vanish at the points $y = 0$ and $y = 1$. There is no SL at the borders of the element because the curves at these points do not depend on Δ_{35}. However, when $y \in (0, 1)$ the functions representing the transverse deflection and the rotation angle do depend on Δ_{35} i.e. on α. Hence, there is an "internal" SL and herein this phenomenon will be designated as FL.

The FL is also observed in the FC: case **2e** (Eq. (46b)) if $M \neq 0$ and case **3e** (Eq. (47b)) if $M \neq 0$ or $P \neq 0$. Although u_{1e} and u_{2e} are independent of Δ_{35} (Eqs. (46a) and (47a)), what matters physically are the "final" curves and not the "intermediate" expansion coefficients.

It is remarkable that the FC is "more sensitive" to the moment M than to the force P (case **2e**). Note that the effective shear force and bending moment are calculated with the integrals

$$Q_y(x) = \int_x^L p(x')\,\mathrm{d}x' \tag{51a}$$

$$M_z(x) = \int_x^L \left[m(x') + Q_y(x')\right]\mathrm{d}x' \tag{51b}$$

and then the transverse deflection and rotation angle are determined by solving the Euler–Lagrange equations

$$\frac{\mathrm{d}w}{\mathrm{d}x} - \beta = \frac{Q_y(x)}{kAG} \tag{52a}$$

$$\frac{\mathrm{d}\beta}{\mathrm{d}x} = \frac{M_z(x)}{EI} \tag{52b}$$

In the FC the curves w and β are approximated by polynomials of degree three and two respectively. Hence, the left side of Eq. (52a) is a polynomial of degree two and the left side of Eq. (52b) is a polynomial of degree one. There are less degrees of freedom to fit M_z than to fit Q_y. In this way, the phenomenon of FL which is associated with low order interpolation, manifests stronger in Eq. (51b) (where both M and P contribute) than in Eq. (51a) (where only P contributes).

There is no FL in the MI (Eqs. (40b) and (42b)) and in the DSG (Eqs. (49b) and (50b)). Observe that in the MI $\gamma_{d*} = \gamma_d$ for $y = \frac{1}{6}$, $y = \frac{1}{2}$, $y = \frac{5}{6}$ (the tie points) and in the DSG $\gamma_{f*} = \gamma_f$ for $y = \frac{1}{2}\left[1 - \frac{\sqrt{5}}{3}\right]$, $y = \frac{1}{2}$, $y = \frac{1}{2}\left[1 + \frac{\sqrt{5}}{3}\right]$. This suggests that the DSG is equivalent to the MI with tie points at $\xi'_{1*} = -\frac{\sqrt{5}}{3}$, $\xi'_{2*} = 0$, and $\xi'_{3*} = \frac{\sqrt{5}}{3}$. Indeed, the stiffness matrix in the DSG is equal to the stiffness matrix which would be obtained in the MI with ξ'_{1*}, ξ'_{2*}, and ξ'_{3*} as tie points.

Graphical comparison. The curves of case **2c** (Eq. (37b)) and of case **2d** (Eq. (40b)) are shown in Figs. 2–4. The NS depends on Δ_{35} only if $P \neq 0$, but in case **3c** (not shown in the figures) the NS also depends on Δ_{35} if $M \neq 0$. When α is small (e.g. $\alpha = 0.1$) the curves become virtually identical ($w_c \approx w_d$ and $\gamma_c \approx \gamma_d \approx \gamma_{d*}$) or at least more similar ($\beta_c \sim \beta_d$). However, for large values of α (e.g. $\alpha = 10$) differences become evident.

The best fitting of the rotation angle in Fig. 3 is the red curve β_d, which corresponds to the MI. But the differences between the exact shear strain and the calculated $\gamma = \mathrm{d}w/\mathrm{d}x - \beta$ (see Fig. 4(*a*)) are bigger for the red curve γ_d than for the blue curve γ_c. Hence, improving the calculation of β in the MI worsens γ.

Observe that γ_{d*} is closer than γ_d to the exact shear strain. The calculated γ_{d*} is the best approximation which can be achieved for the shear strain with polynomials up to the second degree. It gives always the same outcome (independent of α) and so γ_{d*} represents the meaningful shear strain.

Comparing Fig. 3(*a*) and (*b*), it can be seen that only the blue curve depends on the parameter α. This happens because in Eq. (37b) the function multiplying $PL^2/4EI$ contains a term inversely proportional to Δ_{35}, which does not appear in Eq. (40b). A similar conclusion can be drawn for w, but here the ratio between $PL^3/4EI$ and $PL/kAG = PL^3/4\alpha EI$ also depends on α. However, if the functions multiplying PL^3/EI and PL/kAG are considered separately, the shape of the curves varies in the PD but not in the MI. A similar conclusion can be drawn for the FC and for the DSG, where the shape of the curves varies in the FC but not in the DSG.

3.4. Curved beam

In order to analyze FL in higher dimensions, a two-dimensional curved beam is considered (Fig. 5). In this case, the horizontal displacement w_x and the vertical displacement w_y must be calculated in order to obtain the normal strains

$$\epsilon_{xx} = \frac{\partial w_x}{\partial x} \quad \epsilon_{yy} = \frac{\partial w_y}{\partial y}$$

and the shear strain

$$\gamma = 2\epsilon_{xy} = \frac{\partial w_y}{\partial x} + \frac{\partial w_x}{\partial y}$$

Using the same Lagrange basis $\mathcal{F}_4 = \{f_{ci}\}$ as in Section 3.3.1, the displacements can be written as

$$w_x(\xi, \zeta) = \sum_{i=2,3,4} \left(w_{xi} - \zeta\beta_i \frac{b}{2}\sin\theta_i\right) f_{ci}(\xi)$$

$$w_y(\xi, \zeta) = \sum_{i=2,3,4} \left(w_{yi} + \zeta\beta_i \frac{b}{2}\cos\theta_i\right) f_{ci}(\xi) \tag{53}$$

where $\theta_2 = 15°$, $\theta_3 = 30°$, and $\theta_4 = 45°$. The coordinate $\xi \in [-1, 1]$ is tangent to the neutral axis of the beam and the coordinate $\zeta \in [-1, 1]$ is in the radial (orthogonal) direction.

The purpose of the calculation is to determine the coefficients of the expansion w_{xi}, w_{yi}, β_i ($i = 2, 3, 4$) and the details can be found e.g. in Bathe (1996). In particular, in order to mimic the analytic results of the previous sections, the element was divided in a 15 × 15 mesh of quadrilaterals. Each one was integrated using a 4 × 4 Gaussian quadrature, i.e. the calculations avoid the reduced integration. The

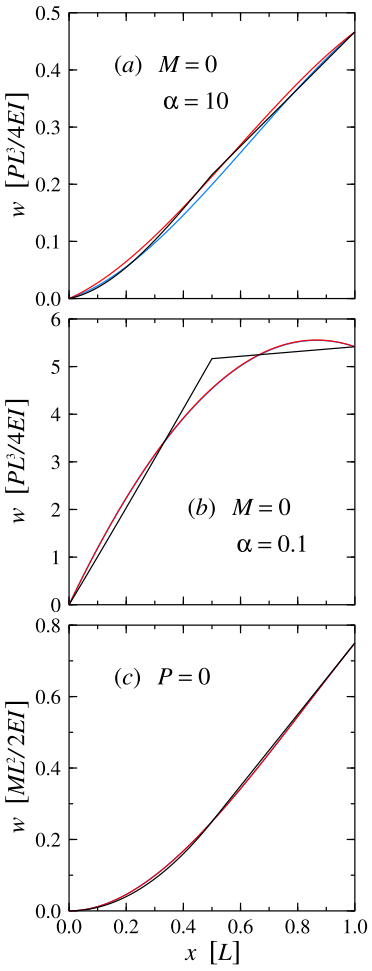

Fig. 2. Transverse deflection as function of x for different values of α. In (a), (b) only a force P is applied and in (c) only a moment M is applied. The black curve is the ES, the blue curve w_c corresponds to the solution obtained with the PD (case **2c**), and the red curve w_d corresponds to the solution obtained with the MI (case **2d**). In (b) and (c) the red curve overshadows the blue curve. (For interpretation of the references to color in this figure legend, the reader is referred to the web version of this article.)

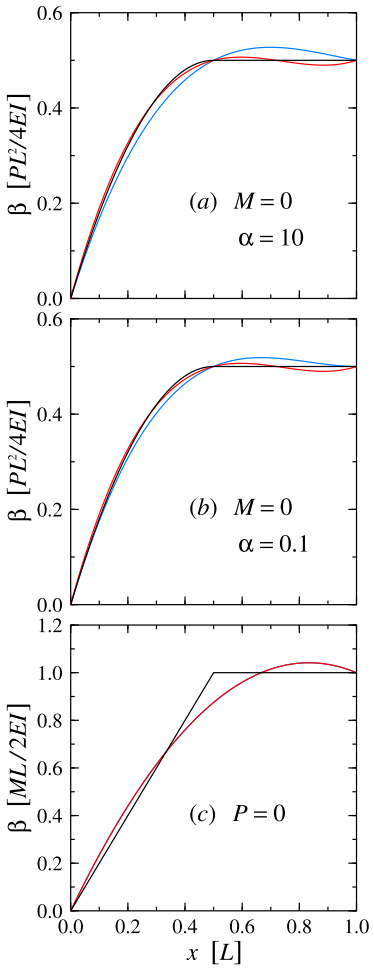

Fig. 3. Same as in Fig. 2 but for the rotation angle. In (c) the red curve overshadows the blue curve. (For interpretation of the references to color in this figure legend, the reader is referred to the web version of this article.)

relevant parameters employed in the numerical calculations are the Poisson ratio $\nu = 0.3$ and the shear correction factor $k = 5/6$ which corresponds to a rectangular cross section.

In the one-dimensional beam, when there is FL, the ratios u_{c1}/u_{d1}, u_{c2}/u_{d2}, u_{c4}/u_{d4}, and u_{c5}/u_{d5} between the coefficient in the PD approach (Eqs. (37a), (38a)) and the coefficient in the MI approach (Eqs. (40a), (42a)) depend on the thickness, especially as the beam becomes thin. Note that in all cases $u_{c3}/u_{d3} = u_{c6}/u_{d6} = 1$, which means that the ratio of the coefficients determining the deformation at the tip cannot be used to conclude if there is FL. Furthermore, if the NS coincides with the ES (as in cases **1c** and **1d**), all ratios are equal to one because both approaches give the same outcome. Finally, FL appears whenever the coefficients contain the term $1/\Delta_\eta$. This will be the case in Eq. (37a) if $P \neq 0$ and the case in Eq. (38a) if $P \neq 0$ or $M \neq 0$. Hence, FL is more sensitive to force loads than to moment loads.

Figs. 6–9 show the ratios between the calculated coefficients for the curved beam. The thickness b varies from 0.001ρ to 0.5ρ, where ρ represents the beam radius. In Figs. 6 and 7, the moment and the force, respectively, are applied at the tip and it is the two-dimensional analogous of cases **1c**, **1d**. In Figs. 8 and 9, the moment and the force, respectively, are applied at the center and it is the two-dimensional analogous of cases **2c**, **2d**.

In general, the blue curve in Figs. 6–9 (associated with the displacements at the tip) has the closest value to one. However, for $b < 10^{-2}\rho$ locking also becomes evident at the tip, showing that in the two-dimensional case locking is more severe (there can be SL and membrane locking). Furthermore, the red curve (associated with the second node located at $\theta_2 = 15°$) always displays the strongest decrease at $b \sim 10^{-3}\rho$. It is important to highlight that in Fig. 9 the ratios depend on the thickness even at moderate values $b \sim 10^{-1}\rho$. Comparing Fig. 8 with Fig. 9, it can be concluded that FL is more sensitive to force than to moment loads, as pointed previously in the one-dimensional case.

In summary, when the thickness becomes large, the calculations performed within the PD approach and within the MI approach give similar results. However, when the beam becomes thin, the coefficients calculated within the PD approach are smaller, giving rise to FL. In this case, the second node shows the most significant reduction of the displacements.

3.5. Necessary and sufficient conditions

Assuming a general structure for the stiffness matrices, it will now be analyzed under what conditions a solution of the form found in the PD and of the form found in the MI can be obtained. Strikingly, the PD contains the MI as a special case.

Mixed interpolation. In general, using a basis $\mathcal{F}_N$ of degree N_1, the linear system to be solved can be written as (see Section 2.3 and Eq. (30) for an example)

$$\begin{pmatrix} \alpha \mathsf{A} & \alpha \mathsf{B}_\mathrm{m} \\ \alpha \mathsf{B}_\mathrm{m}^T & \mathsf{A} + \alpha \mathsf{C}_\mathrm{m} \end{pmatrix} \hat{\mathsf{u}}_\alpha = \begin{pmatrix} \mathsf{a} \\ \mathsf{b} \end{pmatrix} \tag{54a}$$

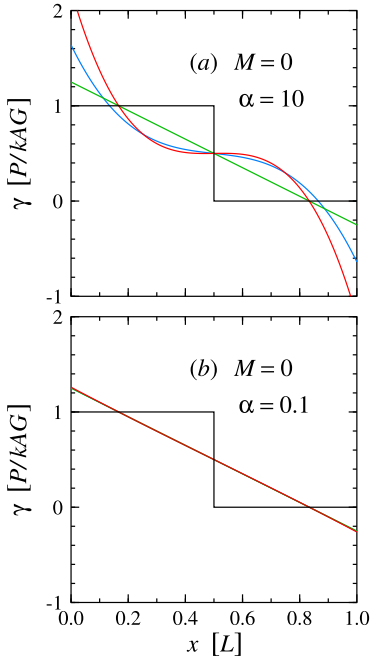

Fig. 4. Shear strain as function of x. The green, red, and blue curves correspond to γ_{d*}, γ_d, and γ_c respectively. In (b) the red curve overshadows the blue and green curves. (For interpretation of the references to color in this figure legend, the reader is referred to the web version of this article.)

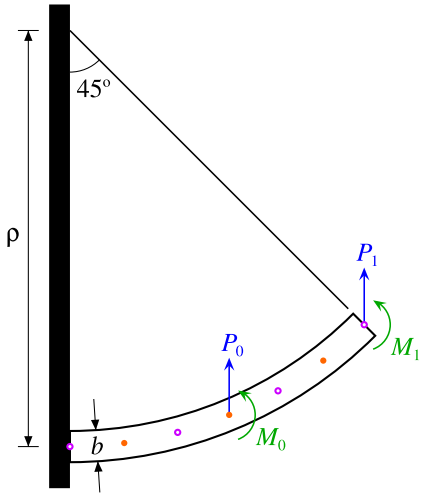

Fig. 5. Curved beam of radius ρ and thickness b. The moment M_0 (M_1) and the vertical force P_0 (P_1) are applied at the center (tip) of the beam. The open magenta dots represent the position of the nodes which are numbered from $i = 1$ to 4 from left to right. The solid orange dots represent the position of the tie points used in the MI.

The proposed solution to the system is

$$\hat{u}_\alpha = \begin{pmatrix} x_1 + \alpha^{-1} y \\ x_2 \end{pmatrix} \tag{54b}$$

so that

$$\begin{aligned} &\alpha(Ax_1 + B_m x_2) + Ay = a \\ &\alpha(B_m^T x_1 + C_m x_2) + B_m^T y + Ax_2 = b \end{aligned} \tag{55}$$

The vectors in Eq. (55) are of dimension N_1, because the components w_1 and β_1 are equal to zero and have been eliminated from the problem. Also, the matrices A and C_m are symmetric.

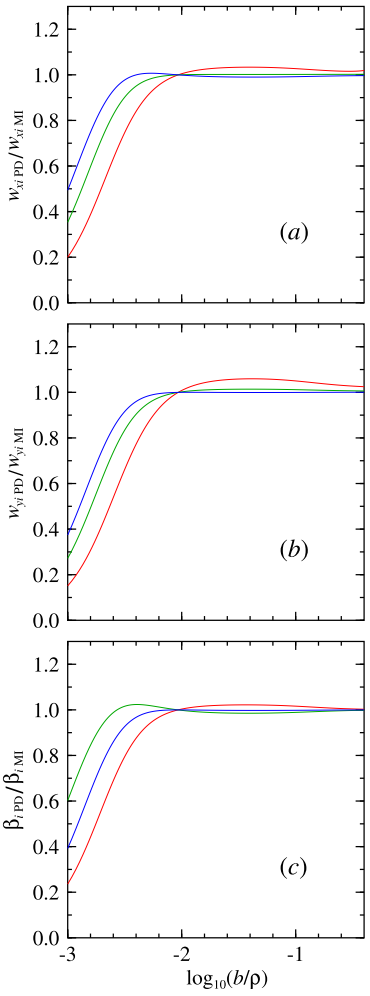

Fig. 6. Curved beam with a moment M_1 applied at the tip (see Fig. 5). The ratios of the coefficients (a) w_{xi}, (b) w_{yi}, (c) β_i in the PD approach and in the MI approach are given as function of the logarithm of the element slenderness b/ρ. The red, green, and blue lines correspond to $i = 2$, $i = 3$, and $i = 4$, respectively. (For interpretation of the references to color in this figure legend, the reader is referred to the web version of this article.)

The question to be answered is whether the general solution $\hat{u}_\alpha$ has the form proposed in Eq. (54b) for arbitrary inputs α, a, and b. From Eq. (55) it follows that

$$Ax_1 + B_m x_2 = 0 \quad \Rightarrow \quad x_1 = -A^{-1} B_m x_2 \tag{56a}$$

$$Ay = a \quad \Rightarrow \quad y = A^{-1} a \tag{56b}$$

$$B_m^T x_1 + C_m x_2 = 0 \quad \Rightarrow \quad (C_m - B_m^T A^{-1} B_m) x_2 = 0 \tag{56c}$$

$$B_m^T y + Ax_2 = b \quad \Rightarrow \quad x_2 = A^{-1}(b - B_m^T A^{-1} a) \tag{56d}$$

Eq. (56c) must be valid for any x_2 because a and b in Eq. (56d) are arbitrary. Hence,

$$C_m = B_m^T A^{-1} B_m \tag{57}$$

Note that the matrices A, B_m, and C_m are determined solely by the integral of $f_\gamma f_\gamma^T$ which is associated with the shear energy. If Eq. (57) is satisfied, then Eq. (54b) reads explicitly

$$\hat{u}_\alpha = \begin{pmatrix} A^{-1} B_m A^{-1} B_m^T A^{-1} + \alpha^{-1} A^{-1} & -A^{-1} B_m A^{-1} \\ -A^{-1} B_m^T A^{-1} & A^{-1} \end{pmatrix} \begin{pmatrix} a \\ b \end{pmatrix} \tag{58}$$

showing that Eq. (57) is not only necessary but also sufficient.

By performing explicit calculations of A, B_m, and C_m up to $N_1 = 30$, it has been verified that the matrices in the MI satisfy Eq. (57).

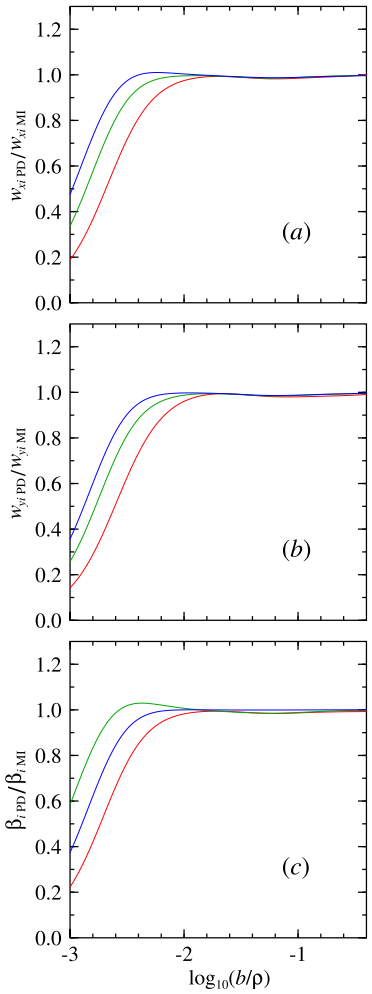

Fig. 7. It is similar to Fig. 6 but with a force P_1 applied at the tip (see Fig. 5).

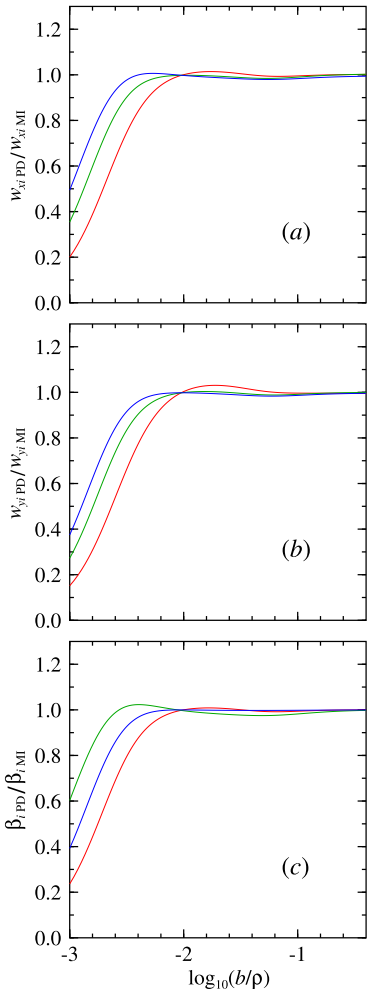

Fig. 8. It is similar to Fig. 6 but with a moment M_0 applied at the center (see Fig. 5).

Furthermore, the stiffness matrix in the DSG also has the form displayed in Eq. (54a) and the Eq. (57) is satisfied again. Finally, the matrix in the FC is

$$\mathsf{K} = \frac{EI}{L\Delta_3}\begin{pmatrix} \alpha & -\alpha \\ -\alpha & 1+\frac{4\alpha}{3} \end{pmatrix} \tag{59a}$$

which is different from Eq. (54a) because of the division by Δ_3. However, the inverse matrix is

$$\mathsf{K}^{-1} = \frac{L}{EI}\begin{pmatrix} \frac{1}{\alpha}+\frac{4}{3} & 1 \\ 1 & 1 \end{pmatrix} \tag{59b}$$

and so the general solution coincides with Eq. (54b). In summary, the coefficients in the MI, in the DSG, and in the FC do not show locking.

Pure displacement. The linear system to be solved is identical to Eq. (54a)

$$\begin{pmatrix} \alpha\mathsf{A} & \alpha\mathsf{B}_\mathrm{p} \\ \alpha\mathsf{B}_\mathrm{p}^T & \mathsf{A}+\alpha\mathsf{C}_\mathrm{p} \end{pmatrix}\hat{\mathsf{u}}_\delta = \begin{pmatrix} \mathsf{a} \\ \mathsf{b} \end{pmatrix} \tag{60a}$$

Note that the matrix A in the upper left corner is the same as in the lower right corner, because the first N functions in the vector $\mathsf{g}_w - \mathsf{f}_\beta$ are equal to the last N functions in the vector g_β (see Eqs. (3a) and (3b)). Furthermore, since the lower right corner is calculated with the same basis functions g_β in the PD and in the MI, the matrix A in Eq. (54a) is equal to the matrix A in Eq. (60a). However, $\mathsf{B}_\mathrm{p} \neq \mathsf{B}_\mathrm{m}$ and $\mathsf{C}_\mathrm{p} \neq \mathsf{C}_\mathrm{m}$ because, as shown in Section 2.3, $\psi_j(\xi) = \mathrm{d}f_j/\mathrm{d}\xi$ and $\varphi_j(\xi) \neq f_j(\xi)$.

Instead of Eq. (54b), the solution has now the form

$$\hat{\mathsf{u}}_\delta = \begin{pmatrix} \mathsf{x}_1 + \alpha^{-1}\mathsf{y} + \alpha^{-1}\Delta_\eta^{-1}\mathsf{z}_1 \\ \mathsf{x}_2 + \Delta_\eta^{-1}\mathsf{z}_2 \end{pmatrix} \tag{60b}$$

where

$$\eta = 4N_1^2 - 1 \tag{60c}$$

Then

$$\alpha(\mathsf{A}\mathsf{x}_1 + \mathsf{B}_\mathrm{p}\mathsf{x}_2 + \Delta_\eta^{-1}\mathsf{B}_\mathrm{p}\mathsf{z}_2) + \mathsf{A}\mathsf{y} + \Delta_\eta^{-1}\mathsf{A}\mathsf{z}_1 = \mathsf{a}$$
$$\alpha(\mathsf{B}_\mathrm{p}^T\mathsf{x}_1 + \mathsf{C}_\mathrm{p}\mathsf{x}_2 + \Delta_\eta^{-1}\mathsf{C}_\mathrm{p}\mathsf{z}_2) + \mathsf{B}_\mathrm{p}^T\mathsf{y} + \Delta_\eta^{-1}\mathsf{B}_\mathrm{p}^T\mathsf{z}_1 + \mathsf{A}\mathsf{x}_2 + \Delta_\eta^{-1}\mathsf{A}\mathsf{z}_2 = \mathsf{b}$$

and upon multiplication by $\eta\Delta_\eta = \eta + \alpha$

$$\alpha^2(\mathsf{A}\mathsf{x}_1 + \mathsf{B}_\mathrm{p}\mathsf{x}_2) + \alpha(\eta\mathsf{A}\mathsf{x}_1 + \eta\mathsf{B}_\mathrm{p}\mathsf{x}_2 + \eta\mathsf{B}_\mathrm{p}\mathsf{z}_2 + \mathsf{A}\mathsf{y}) + \eta\mathsf{A}\mathsf{y} + \eta\mathsf{A}\mathsf{z}_1 = \alpha\mathsf{a} + \eta\mathsf{a}$$
$$\alpha^2(\mathsf{B}_\mathrm{p}^T\mathsf{x}_1 + \mathsf{C}_\mathrm{p}\mathsf{x}_2) + \alpha(\eta\mathsf{B}_\mathrm{p}^T\mathsf{x}_1 + \eta\mathsf{C}_\mathrm{p}\mathsf{x}_2 + \eta\mathsf{C}_\mathrm{p}\mathsf{z}_2 + \mathsf{B}_\mathrm{p}^T\mathsf{y} + \mathsf{A}\mathsf{x}_2)$$
$$+ \eta\mathsf{B}_\mathrm{p}^T\mathsf{y} + \eta\mathsf{B}_\mathrm{p}^T\mathsf{z}_1 + \eta\mathsf{A}\mathsf{x}_2 + \eta\mathsf{A}\mathsf{z}_2 = \alpha\mathsf{b} + \eta\mathsf{b}$$

Since α is arbitrary

$$\mathsf{A}\mathsf{x}_1 + \mathsf{B}_\mathrm{p}\mathsf{x}_2 = 0$$
$$\eta(\mathsf{A}\mathsf{x}_1 + \mathsf{B}_\mathrm{p}\mathsf{x}_2 + \mathsf{B}_\mathrm{p}\mathsf{z}_2) + \mathsf{A}\mathsf{y} = \mathsf{a}$$
$$\mathsf{A}(\mathsf{y} + \mathsf{z}_1) = \mathsf{a}$$
$$\mathsf{B}_\mathrm{p}^T\mathsf{x}_1 + \mathsf{C}_\mathrm{p}\mathsf{x}_2 = 0$$
$$\eta(\mathsf{B}_\mathrm{p}^T\mathsf{x}_1 + \mathsf{C}_\mathrm{p}\mathsf{x}_2 + \mathsf{C}_\mathrm{p}\mathsf{z}_2) + \mathsf{B}_\mathrm{p}^T\mathsf{y} + \mathsf{A}\mathsf{x}_2 = \mathsf{b}$$
$$\mathsf{B}_\mathrm{p}^T(\mathsf{y} + \mathsf{z}_1) + \mathsf{A}(\mathsf{x}_2 + \mathsf{z}_2) = \mathsf{b}$$

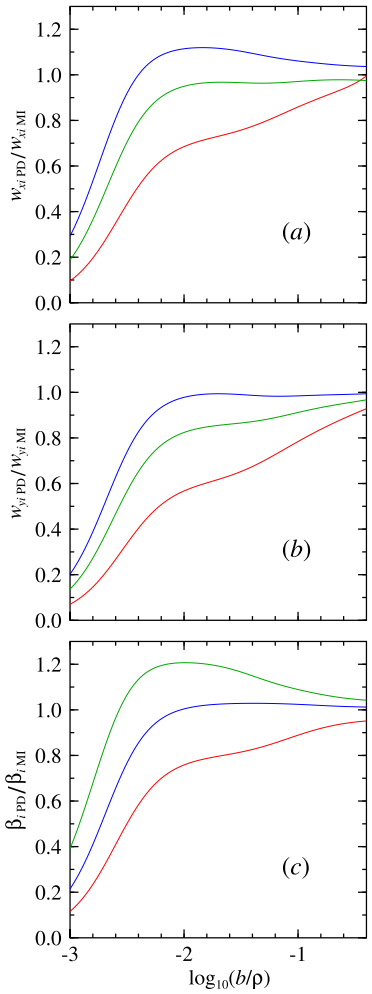

Fig. 9. It is similar to Fig. 6 but with a force P_0 applied at the center (see Fig. 5).

and simplifying

$$\mathsf{x}_1 = -\mathsf{A}^{-1}\mathsf{B}_\mathrm{p}\mathsf{x}_2 \tag{61a}$$

$$\mathsf{y} = \mathsf{A}^{-1}(\mathsf{a} - \eta\mathsf{B}_\mathrm{p}\mathsf{z}_2) \tag{61b}$$

$$\mathsf{z}_1 = \eta\mathsf{A}^{-1}\mathsf{B}_\mathrm{p}\mathsf{z}_2 \tag{61c}$$

$$(\mathsf{C}_\mathrm{p} - \mathsf{B}_\mathrm{p}^T\mathsf{A}^{-1}\mathsf{B}_\mathrm{p})\mathsf{x}_2 = 0 \tag{61d}$$

$$\mathsf{A}\mathsf{x}_2 + \eta(\mathsf{C}_\mathrm{p} - \mathsf{B}_\mathrm{p}^T\mathsf{A}^{-1}\mathsf{B}_\mathrm{p})\mathsf{z}_2 = \mathsf{b} - \mathsf{B}_\mathrm{p}^T\mathsf{A}^{-1}\mathsf{a} \tag{61e}$$

$$\mathsf{A}\mathsf{x}_2 + \mathsf{A}\mathsf{z}_2 = \mathsf{b} - \mathsf{B}_\mathrm{p}^T\mathsf{A}^{-1}\mathsf{a} \tag{61f}$$

It was shown in Section 2.2 that the inverse of A always exists, but it can be verified that B_p and C_p do not have an inverse except for $N_1 = 1$. Eqs. (61a), (61b), and (61c) determine x_1, y, and z_1 as function of x_2 and z_2. From Eqs. (61e) and (61f) it follows that

$$\mathsf{D}\mathsf{z}_2 = \frac{1}{\eta}\mathsf{z}_2 \tag{62a}$$

with

$$\mathsf{D} = \mathsf{A}^{-1}(\mathsf{C}_\mathrm{p} - \mathsf{B}_\mathrm{p}^T\mathsf{A}^{-1}\mathsf{B}_\mathrm{p}) \tag{62b}$$

According to Eq. (62a), z_2 must be an eigenvector of the matrix D with eigenvalue η^{-1}. If $\mathsf{C}_\mathrm{p} = \mathsf{B}_\mathrm{p}^T\mathsf{A}^{-1}\mathsf{B}_\mathrm{p}$, then D = 0, $\mathsf{z}_2 = 0$, and $\mathsf{z}_1 = 0$, i.e. the solution becomes identical to the MI given previously.

From Eq. (61f) it follows that

$$\mathsf{x}_2 = \mathsf{d} - \mathsf{z}_2 \tag{63a}$$

Table 1
Values of η and vectors v_1, v_2, v_3 for the firsts N_1.

(a)	$N_1 = 1$ $\eta = 3$	$\mathsf{v}_1^T = (1)$ $\mathsf{v}_2^T = (1)$ $\mathsf{v}_3^T = (-3)$
(b)	$N_1 = 2$ $\eta = 15$	$\mathsf{v}_1^T = (-2 \quad 1)$ $\mathsf{v}_2^T = \left(-\frac{1}{2} \quad 0\right)$ $\mathsf{v}_3^T = (5 \quad 10)$
(c)	$N_1 = 3$ $\eta = 35$	$\mathsf{v}_1^T = (3 \quad -3 \quad 1)$ $\mathsf{v}_2^T = \left(\frac{1}{6} \quad -\frac{1}{6} \quad 0\right)$ $\mathsf{v}_3^T = \left(-\frac{7}{2} \quad -\frac{7}{2} \quad 0\right)$
(d)	$N_1 = 4$ $\eta = 63$	$\mathsf{v}_1^T = (-4 \quad 6 \quad -4 \quad 1)$ $\mathsf{v}_2^T = \left(-\frac{1}{40} \quad \frac{2}{15} \quad -\frac{1}{40} \quad 0\right)$ $\mathsf{v}_3^T = \left(\frac{9}{5} \quad 0 \quad -\frac{9}{5} \quad 0\right)$
(e)	$N_1 = 5$ $\eta = 99$	$\mathsf{v}_1^T = (5 \quad -10 \quad 10 \quad -5 \quad 1)$ $\mathsf{v}_2^T = \left(-\frac{3}{140} \quad -\frac{17}{280} \quad \frac{17}{280} \quad \frac{3}{140} \quad 0\right)$ $\mathsf{v}_3^T = \left(-\frac{55}{84} \quad \frac{55}{56} \quad \frac{55}{56} \quad -\frac{55}{84} \quad 0\right)$
(f)	$N_1 = 6$ $\eta = 143$	$\mathsf{v}_1^T = (-6 \quad 15 \quad -20 \quad 15 \quad -6 \quad 1)$ $\mathsf{v}_2^T = \left(\frac{29}{1008} \quad \frac{4}{315} \quad -\frac{27}{560} \quad \frac{4}{315} \quad \frac{29}{1008} \quad 0\right)$ $\mathsf{v}_3^T = \left(\frac{13}{252} \quad -\frac{52}{63} \quad 0 \quad \frac{52}{63} \quad -\frac{13}{252} \quad 0\right)$

with

$$\mathsf{d} = \mathsf{A}^{-1}(\mathsf{b} - \mathsf{B}_\mathrm{p}^T\mathsf{A}^{-1}\mathsf{a}) \tag{63b}$$

Substituting x_2 into Eq. (61d) gives

$$(\mathsf{C}_\mathrm{p} - \mathsf{B}_\mathrm{p}^T\mathsf{A}^{-1}\mathsf{B}_\mathrm{p})\mathsf{z}_2 = (\mathsf{C}_\mathrm{p} - \mathsf{B}_\mathrm{p}^T\mathsf{A}^{-1}\mathsf{B}_\mathrm{p})\mathsf{d}$$

and multiplying by $\eta\mathsf{A}^{-1}$

$$\mathsf{z}_2 = \eta\mathsf{D}\mathsf{d} \tag{64}$$

where Eqs. (62a), (62b) have been used. If the vector d belongs to the kernel of the matrix D, then $\mathsf{z}_1 = \mathsf{z}_2 = 0$ and there is no locking. Furthermore, substituting Eq. (64) into Eq. (63a)

$$\mathsf{x}_2 = (1 - \eta\mathsf{D})\mathsf{d} \tag{65}$$

From Eqs. (64) and (62a) it follows that

$$\eta\mathsf{D}^2\mathsf{d} = \mathsf{D}\mathsf{d}$$

According to Eq. (63b) the vector d is arbitrary because a and b are arbitrary. Thus, it is necessary that

$$\mathsf{D}^2 = \frac{1}{\eta}\mathsf{D} \tag{66}$$

By performing explicit calculations of D up to $N_1 = 30$, it has been verified that the matrix indeed satisfies Eq. (66).

The inverse matrix A^{-1} and the D matrix are relevant for the determination of z_2, x_2, and subsequent calculations of x_1, y, z_1. In particular, the matrix D can be decomposed in the form

$$\mathsf{D} = \frac{1}{\eta}\mathsf{v}_2\mathsf{v}_1^T \tag{67}$$

Table 1 contains the first values of η and the respective vectors v_1, v_2. Note that the scalar product between v_1 and v_2 is

$$\mathsf{v}_1^T\mathsf{v}_2 = 1 \tag{68}$$

Remark that Eqs. (67) and (68) imply Eq. (66). Moreover, multiplying v_1 by a constant and dividing v_2 by the same constant leaves Eqs. (67) and (68) unchanged, i.e. there is one degree of freedom in the determination of v_1 and v_2. The arbitrary constant has been chosen so that the last component of v_1 is equal to one.

The result of $\mathsf{D}\mathsf{z}_2 = \eta^{-1}\mathsf{v}_2(\mathsf{v}_1^T\mathsf{z}_2)$ is a vector parallel to v_2. Additionally, Eq. (62a) implies that the vector v_2 must be parallel to z_2. If $\mathsf{v}_\perp$ represents a vector perpendicular to v_1, then $\mathsf{D}\mathsf{v}_\perp = 0$, i.e. $\mathsf{v}_\perp$ belongs

to the kernel of D. Since the dimension of v_1 is N_1, the number of LI vectors perpendicular to v_1 is $N_1 - 1$. Thus the dimension of the kernel is $N_1 - 1$ and for $N_1 > 1$ the matrix D has no inverse. This is consistent with the fact that the last component of v_2 vanishes and so the last line of D is equal to zero. Moreover, the last component of z_2 also vanishes because it is parallel to the vector v_2. Hence, the rotation angle β does not shear lock at $x = L$ if $N_1 > 1$, i.e. if the element has more than two nodes. In this case, β is approximated by a polynomial of degree two or larger. In the specific case of $N_1 = 1$, it has been explicitly shown in Eq. (23) that β_{a2} locks (the "last line" of the matrix $\mathsf{D} = \frac{1}{3}\mathsf{v}_2\mathsf{v}_1^T = \left(\frac{1}{3}\right)$ is different from zero).

It is also interesting to investigate the properties of z_1, because this vector is related to the locking of w_i in the same way as z_2 is related to the locking of β_i. From Eqs. (61c) and (64)

$$\mathsf{z}_1 = \eta^2 \mathsf{E}\mathsf{d} \tag{69a}$$

where

$$\mathsf{E} = \mathsf{A}^{-1}\mathsf{B}_\mathrm{p}\mathsf{D} \tag{69b}$$

It can be verified that the matrix E can be decomposed in the following form (see Table 1)

$$\mathsf{E} = \frac{1}{\eta^2}\mathsf{v}_3\mathsf{v}_1^T \tag{70}$$

and for $N_1 > 1$

$$\mathsf{v}_1^T\mathsf{v}_3 = 0 \tag{71}$$

Hence, E^2 coincides with the null matrix.

The vector $\mathsf{z}_1 = \mathsf{v}_3(\mathsf{v}_1^T\mathsf{d})/\eta^2$ is parallel to v_3. One important point is that the last component of v_3 is equal to zero for $N_1 > 2$ and so the last component of z_1 is zero. Hence, the transverse deflection w does not shear lock at $x = L$ if $N_1 > 2$, i.e. if the element has more than three nodes. In this case, w is approximated by a polynomial of degree three or larger.

3.6. Generalizations to multiple elements

First, general aspects of the NS are discussed for increasing number of elements. Then the decomposition of the matrices D and E of the PD is taken into account and, in particular, it will be analyzed when locking occurs.

Consider the instance where the beam is divided into $N_\mathrm{e} = 2$ elements. If the calculations corresponding to the tip load (Fig. 1(*a*)) are performed using third order polynomials (i.e. $N = 4$ nodes per element), then the NS coincides with the ES. The same result is also found for the center load (Fig. 1(*b*)). In particular, FL is suppressed in the PD. The key point is that one set of polynomials of degree three is sufficient to match the ES in the interval $0 < x < L/2$, and another set of polynomials of degree three is sufficient to match the ES in the interval $L/2 < x < L$. However, in the off-center load (Fig. 1(*c*)) the ES is not an analytic function at $x = L/3$. The NS coincides with the ES in the interval $L/2 < x < L$, but they are different in the interval $0 < x < L/2$.

The analysis can be extended to a higher number of elements. For example, with $N_\mathrm{e} = 3$ elements and considering the tip load, the NS coincides with the ES. However, in the center load the ES is not an analytic function at $x = L/2$, and the NS does not coincide with the ES in the interval $L/3 < x < 2L/3$. But even so, in the intervals $0 < x < L/3$ and $2L/3 < x < L$ the NS coincides with the ES. Finally, in the off-center load the NS coincides with the ES in the entire interval $0 < x < L$.

The results of Section 3.5 remain valid if N_1 is substituted by $N_\mathrm{e}N_1$ (the dimension of the vectors and of the matrices increases by the factor N_e). Moreover, Eqs. (67), (70) and Eqs. (68), (71) are replaced by

$$\mathsf{D} = \frac{1}{\eta}\sum_{i=1}^{N_\mathrm{e}} \mathsf{v}_{2i}\mathsf{v}_{1i}^T \tag{72a}$$

$$\mathsf{E} = \frac{1}{\eta^2}\sum_{i=1}^{N_\mathrm{e}} \mathsf{v}_{3i}\mathsf{v}_{1i}^T \tag{72b}$$

and

$$\mathsf{v}_{1i}^T\mathsf{v}_{2j} = \delta_{ij} \tag{73a}$$

$$\mathsf{v}_{1i}^T\mathsf{v}_{3j} = 0 \tag{73b}$$

respectively. However, when $N_1 < 3$ Eq. (72b) does not hold. Indeed, if $N_\mathrm{e} = 3$ elements and $N = 3$ nodes per element, then $N_1 = 2$, $\eta = 15$, and

$$\mathsf{E} = \begin{pmatrix} -\frac{2}{45} & \frac{1}{45} & 0 & 0 & 0 & 0 \\ -\frac{4}{45} & \frac{2}{45} & 0 & 0 & 0 & 0 \\ -\frac{4}{45} & \frac{1}{45} & -\frac{2}{45} & \frac{1}{45} & 0 & 0 \\ -\frac{4}{45} & \frac{4}{45} & -\frac{4}{45} & \frac{2}{45} & 0 & 0 \\ -\frac{4}{45} & \frac{4}{45} & -\frac{4}{45} & \frac{1}{45} & -\frac{2}{45} & \frac{1}{45} \\ -\frac{4}{45} & \frac{4}{45} & -\frac{4}{45} & \frac{4}{45} & -\frac{4}{45} & \frac{2}{45} \end{pmatrix} \tag{74}$$

which cannot be decomposed in the form of Eq. (72b).

As an example where Eqs. (72a)–(73b) hold, consider $N_\mathrm{e} = 3$ elements and $N = 4$ nodes per element. Then $N_1 = 3$, $\eta = 35$, and the vectors are

$$\begin{aligned}
\mathsf{v}_{11}^T &= \begin{pmatrix} 3 & -3 & 1 & 0 & 0 & 0 & 0 & 0 & 0 \end{pmatrix} \\
\mathsf{v}_{21}^T &= \begin{pmatrix} \frac{1}{6} & -\frac{1}{6} & 0 & 0 & 0 & 0 & 0 & 0 & 0 \end{pmatrix} \\
\mathsf{v}_{31}^T &= \begin{pmatrix} -\frac{7}{2} & -\frac{7}{2} & 0 & 0 & 0 & 0 & 0 & 0 & 0 \end{pmatrix} \\
\mathsf{v}_{12}^T &= \begin{pmatrix} 0 & 0 & -1 & 3 & -3 & 1 & 0 & 0 & 0 \end{pmatrix} \\
\mathsf{v}_{22}^T &= \begin{pmatrix} 0 & 0 & 0 & \frac{1}{6} & -\frac{1}{6} & 0 & 0 & 0 & 0 \end{pmatrix} \\
\mathsf{v}_{32}^T &= \begin{pmatrix} 0 & 0 & 0 & -\frac{7}{2} & -\frac{7}{2} & 0 & 0 & 0 & 0 \end{pmatrix} \\
\mathsf{v}_{13}^T &= \begin{pmatrix} 0 & 0 & 0 & 0 & 0 & -1 & 3 & -3 & 1 \end{pmatrix} \\
\mathsf{v}_{23}^T &= \begin{pmatrix} 0 & 0 & 0 & 0 & 0 & 0 & \frac{1}{6} & -\frac{1}{6} & 0 \end{pmatrix} \\
\mathsf{v}_{33}^T &= \begin{pmatrix} 0 & 0 & 0 & 0 & 0 & 0 & -\frac{7}{2} & -\frac{7}{2} & 0 \end{pmatrix}
\end{aligned} \tag{75}$$

Note that the first three components of v_{11}, v_{21}, and v_{31} are equal to the components of v_1, v_2, and v_3 in Table 1(*c*), respectively.

It can be observed that there is a pattern between the v_{1i} vectors and also a pattern between the v_{2i} vectors. In general, the components of v_{1i} different from zero coincide with the coefficients of $a^j b^{N_1-j}$ in the binomial expansion of $(a-b)^{N_1}$

$$\frac{N_1!}{j!\,(N_1-j)!}(-1)^{N_1-j}$$

However, in v_{11} the first component ($j = 0$) should be equal to -1, but it is missing. This happens because the components w_1 and β_1 have been dropped out from the $\hat{\mathsf{u}}$ vector. Hence, two components are removed from the force–moment vector, as well as two lines and two columns are removed from the stiffness matrix. The dimension of the original matrices A, B_p, and C_p decreases by one, and this is the missing component in the vectors v_{1i} and v_{2i}. In order to recover the "full pattern", the calculations could be repeated without removing the first line and the first column of the original matrices A, B_p, and C_p. Nevertheless, the matrix A becomes singular (see Section 2.2) and the matrix D does not exist.

Another interesting point is that the 3rd, 6th, and 9th components of the vectors v_{2i} and v_{3i} are zero. Then there are only zeros in the 3rd, 6th, and 9th lines of the matrices D and E. Hence, the corresponding components of the z_2 and of the z_1 vectors are zero, which means that β and w do not shear lock at the boundary between the elements.

In general, β does not shear lock at the boundary if $N_1 > 1$, i.e. with polynomials of degree two or larger. Also, w does not shear lock at the boundary if $N_1 > 2$, i.e. with polynomials of degree three or larger. On the other hand, in the internal nodes there can be SL.

Conjectures. Some results in the previous sections have been stated but no proof has been given. They include:

- The formula for η (Eq. (60c)).
- The decomposition of the matrices D and E (Eqs. (72a) and (72b)).

These results have been established by performing explicit calculations with N_1 up to 30 and with N_e up to 5.

4. Conclusions

The shape of the curves representing the transverse deflection and the rotation angle in the PD and in the FC depend on the value of $\alpha = kAGL^2/4EI$, which represents the ratio between the strain and the bending energies. The FL is characterized by the presence of the denominator $\Delta_\eta = 1+\alpha/\eta$ in the curves. Locking effects can be detected by analyzing the curves, but they are not evident if only the borders of the elements are studied.

In the PD, the coefficients u_{ci} depend on Δ_η but the basis functions are independent of Δ_η. In the FC, the coefficients u_{ei} are independent of Δ_η but the basis functions depend on Δ_η. The locking is transferred from the coefficients in the PD to the basis functions in the FC. Neither the PD (when $N > 3$ nodes) nor the FC exhibit SL at the borders of the element.

Combining the coefficients and basis functions results in FL both in the PD and in the FC. In particular, FL is observed in case **2e** (center load) if $M \neq 0$ and in case **3e** (off-center load) if $M \neq 0$ or $P \neq 0$. Thus, the FC shows a better performance with force loads than with moment loads.

The DSG is equivalent to the MI but with different tie points, and no one shows FL. When $\gamma_* \neq \gamma$ the virtual shear strain gives a better approach to the exact shear strain. The outcomes with the MI are better than with the PD, because using γ_* in place of γ lowers the shear strain energy and locking becomes less relevant. Furthermore, the degree of the polynomial γ_* decreases by one, and there are more degrees of freedom to match the w- and the β-curves.

The necessary and sufficient condition that the matrices must fulfill in order to have the proposed solution in the MI (Eq. (54b)) and in the PD (Eq. (60b)), have been obtained (Eqs. (57) and (66) respectively). In both cases, the condition depends solely on the matrix associated with the shear strain energy. In particular, it has been confirmed that locking is never observed at the borders of the elements when the polynomial degree of w is at least three and when the polynomial degree of β is at least two.

Declaration of competing interest

The authors declare that they have no known competing financial interests or personal relationships that could have appeared to influence the work reported in this paper.

Acknowledgments

This work was supported by Conselho Nacional de Desenvolvimento Científico e Tecnológico, Brazil (CNPq, project 465586/2014-7).

References

Arroyo, M., Ortiz, M., 2006. Local maximum-entropy approximation schemes: a seamless bridge between finite elements and meshfree methods. Internat. J. Numer. Methods Engrg. 65, 2167–2202.

Babuska, I., Suri, M., 1992. Locking effects in the finite element approximation of elasticity problems. Numer. Math. 62, 439–463.

Bathe, K.J., 1996. Finite Element Procedures. Prentice-Hall.

Bazeley, G.P., Cheung, Y.K., Irons, B.M., Zienkiewicz, O.C., 1966. Triangular elements in plate bending - conforming and nonconforming solutions. report AFFDL-TR-66-80 547–576.

Belytschko, T., Krongauz, Y., Organ, D., Fleming, M., Krysl, P., 1996. Meshless methods: an overview and recent developments. Comput. Methods Appl. Mech. Engrg. 139, 3–47.

Bletzinger, K.U., Bischoff, M., Ramm, E., 2000. A unified approach for shear-locking-free triangular and rectangular shell finite elements. Comput. Struct. 75, 321–334.

Carrera, E., de Miguel, A.G., Pagani, A., 2017. Extension of MITC to higher-order beam models and shear locking analysis for compact, thin-walled, and composite structures. Internat. J. Numer. Methods Engrg. 112, 1889–1908.

Cho, J.Y., Atluri, S.N., 2001. Analysis of shear flexible beams, using the meshless local petov-garleking method, based on a locking-free formulation. Eng. Comput. 18, 215–240.

De, S., Bathe, K.J., 2001. Displacement/pressure mixed interpolation in the method of finite spheres. Internat. J. Numer. Methods Engrg. 51, 275–292.

de Sá, J.M.A.C., Jorge, R.M.N., Valente, R.A.F., Areias, P.M.A., 2002. Development of shear locking-free shell elements using an enhanced assumed strain formulation. Internat. J. Numer. Methods Engrg. 53, 1721–1750.

de Souza Neto, E.A., Peric, D., Huang, G.C., Owen, D.R.J., 1995. Remarks on the stability of enhanced strain elements in finite elasticity and elastoplasticity. Numer. Methods Biomed. Eng. 11, 951–961.

Dolbow, J., Belytschko, T., 1998. Volumetric locking in the element free Galerkin method. Internat. J. Numer. Methods Engrg. 46, 925–942.

Dufva, K.E., Sopanen, J.T., Mikkola, A.M., 2005. A two-dimensional shear deformable beam element based on absolute nodal coordinate formulation. J. Sound Vib. 280, 719–738.

Dvorkin, E.N., Bathe, K.J., 1984. A continuum mechanics based four node shell elements for general non-linear analysis. Eng. Comput. 1, 77–88.

Ebel, H., Matikainen, M.K., Hurskainen, V., Mikkola, A., 2017. Higher-order beam elements based on the absolute nodal coordinate formulation for three-dimensional elasticity. Nonlinear Dynam. 88, 1075–1091.

Fox, D.D., Raoult, A., Simo, J.C., 1993. A justification of nonlinear properly invariant plate theories. Arch. Ration. Mech. Anal. 124, 157–199.

Friedman, Z., Kosmatka, J.B., 1993. An improved two-node Timoshenko beam finite element. Comput. Struct. 47, 473–481.

Garcia, O., Fancello, E.A., de Barcellos, C.S., Duarte, C.A., 2000. Hp-clouds in mindlin's thick plate model. Internat. J. Numer. Methods Engrg. 47, 1381–1400.

García-Vallejo, D., Mikkola, A.M., Escalona, J.L., 2007. A new locking-free shear deformable finite element based on absolute nodal coordinates. Nonlinear Dynam. 50, 249–264.

Gerstmayr, J., Irschik, H., 2008. On the correct representation of bending and axial deformation in the absolute nodal coordinate formulation with an elastic line approach. J. Sound Vib. 318, 461–487.

Gerstmayr, J., Matikainen, M., 2006. Analysis of stress and strain in the absolute nodal coordinate formulation. Mech. Based Des. Struct. Mach. 34, 409–430.

Gerstmayr, J., Matikainen, M.K., Mikkola, A.M., 2008. A geometrically exact beam element based on the absolute nodal coordinate formulation. Multibody Syst. Dyn. 20, 359–384.

Gerstmayr, J., Sugiyama, H., Mikkola, A., 2013. Review on the absolute nodal coordinate formulation for large deformation analysis of multibody systems. ASME J. Comput. Nonlinear Dyn. 8, 031016:1–031016:12.

Hughes, T.J.R., Tezduyar, T., 1981. Finite elements based upon mindlin plate theory with particular reference to the four-node bilinear isoparametric element. J. Appl. Mech. 48, 587–596.

Kiendl, J., Auricchio, F., Reali, A., 2018. A displacement-free formulation for the timoshenko beam problem and a corresponding isogeometric collocation approach. Meccanica 53, 1403–1413.

Leitão, V.M.A., Alves, C.J.S., Duarte, C.A. (Eds.), 2007. Advances in Meshfree Techniques. Springer, pp. 123–145.

Liu, W.K., Li, S., Belytschko, T., 1997. Moving least-square reproducing kernel methods (I) methodology and convergence. Comput. Methods Appl. Mech. Engrg. 143, 113–154.

Macneal, R.H., 1978. A simple quadrilateral shell element. Comput. Struct. 8, 175–183.

Macneal, R.H., 1982. Derivation of element stiffness matrices by assumed strain distributions. Nucl. Eng. Des. 70, 3–12.

Malkus, D.S., Hughes, T.J.R., 1978. Mixed finite element methods-reduced and selective integration techniques: a unification of concepts. Comput. Methods Appl. Mech. Engrg. 15, 63–81.

Nachbagauer, K., Gruber, P., Gerstmayr, J., 2013. Multibody Dynamics. In: Computational Methods in Applied Sciences, 28, Springer, pp. 77–96.

Nachbagauer, K., Pechstein, A.S., Irschik, H., Gerstmayr, J., 2011. A new locking-free formulation for planar, shear deformable, linear and quadratic beam finite elements based on the absolute nodal coordinate formulation. Multibody Syst. Dyn. 26, 245–263.

Nguyen-Xuan, H., 2017. A polygonal finite element method for plate analysis. Comput. Struct. 188, 45–62.

Noor, A., Peters, J., 1981. Mixed models and reduced/selective integration displacement models for nonlinear analysis of curved beams. Int. J. Numer. Methods Eng. 17, 615–631.

Oesterle, B., Bieber, S., Sachse, R., Ramm, E., Bischoff, M., 2018. Intrinsically locking-free formulations for isogeometric beam, plate and shell analysis. In: Proceedings in Applied Mathematics and Mechanics, vol. 18, pp. e201800399:1–e201800399:4.

Pantuso, D., Bathe, K.J., 1997. On the stability of mixed finite elements in large strain analysis of incompressible solids. Finite Elem. Anal. Des. 28, 83–104.
Patel, M., Shabana, A.A., 2018. Locking alleviation in the large displacement analysis of beam elements: the strain split method. Acta Mech. 229, 2923–2946.
Polizzotto, C., 2015. From the Euler-Bernoulli beam to the timoshenko one through a sequence of reddy-type shear deformable beam models of increasing order. Eur. J. Mech. A Solids 53, 62–74.
Prathap, G., 1993. The finite element method in structural mechnics. Springer Science & Busines Media.
Reddy, J.N., 1997. On locking-free shear deformable beam finite elements. Comput. Methods Appl. Mech. Engrg. 149, 113–132.
Shabana, A.A., 1997. Definition of the slopes and the finite element absolute nodal coordinate formulation. Multibody Syst. Dyn. 1, 339–348.
Soh, A.K., Cen, S., Long, Y.Q., Long, Z.F., 2001. A new twelve DOF quadrilateral element for analysis of thick and thin plates. Eur. J. Mech. A Solids 20, 299–326.
Soh, A.K., Long, Z.F., Cen, S., 1999. A new nine DOF triangular element for analysis of thick and thin plates. Comput. Mech. 24, 408–417.
Steiner, T., Wriggers, P., Loehnert, S., 2016. A discontinuous Galerkin Finite Element Method for linear elasticity using a mixed integration scheme to circumvent shear-locking. In: Proceedings in Applied Mathematics and Mechanics. vol. 16, pp. 769–770.
Sussman, T., Bathe, K.J., 2014. Spurious modes in geometrically nonlinear small displacement finite elements with incompatible modes. Comput. Struct. 140, 14–22.
Valkeapää, A.I., Yamashita, H., Jayakumar, P., Sugiyama, H., 2015. On the use of elastic middle surface approach in the large deformation analysis of moderately thick shell structures using absolute nodal coordinate formulation. Nonlinear Dynam. 80, 1133–1146.
Veiga, L.B., Lovadina, C., Reali, A., 2012. Avoiding shear locking for the Timoshenko beam problem via isogeometric collocation methods. Comput. Methods Appl. Mech. Engrg. 241–244, 38–51.
Wilson, E.L., Ibrahimbegovic, A., 1990. Use of incompatible displacement models for the calculation of element stiffness and stresses. Finite Elem. Anal. Des. 7, 229–241.
Wilson, E.L., Taylor, R.L., Doherty, W.P., Ghaboussi, J., 1973. Numerical and Computer Methods in Structural Mechanics. Academic Press, pp. 43–57.
Wong, F.T., Sugianto, S., 2017. Study of the discrete shear gap technique in timoshenko beam elements. Civil Eng. Dimens. 19, 54–62.
Wong, F.T., Sulistio, A., Syamsoeyadi, H., 2018. Kriging-based timoshenko beam elements with the discrete shear gap technique. Int. J. Comput. Methods 15, 1850064:1–1850064:27.
Wriggers, P., Reese, S., 1996. A note on enhanced strain methods for large deformations. Comput. Methods Appl. Mech. Engrg. 135, 201–209.
Yunhua, L., 1998. Explanation and elimination of shear locking and membrane locking with field consistence approach. Comput. Methods Appl. Mech. Engrg. 162, 249–269.
Zienkiewicz, O.C., Taylor, R.L., Fox, D.D., 2013a. The Finite Element Method for Solid and Structural Mechanics, 7th Elsevier.
Zienkiewicz, O.C., Taylor, R.L., Too, J.M., 1971. Reduced integration technique in general analysis of plates and shells. Internat. J. Numer. Methods Engrg. 3, 275–290.
Zienkiewicz, O.C., Taylor, R.L., Zhu, J.Z., 2013b. The finite element method: its basis and fundamentals, 7th Elsevier.